Marine Geology 379 (2016) 157–175

Contents lists available at ScienceDirect

Marine Geology

journal homepage: www.elsevier.com/locate/margo

Postglacial mass movements and depositional environments in a high-latitude fjord system – Hardangerfjorden, Western Norway

Benjamin Bellwald *, Berit Oline Hjelstuen, Hans Petter Sejrup, Haflidi Haflidason

Department of Earth Science, University of Bergen, Allégaten 41, N-5007 Bergen, Norway

ARTICLE INFO

Article history:
Received 6 October 2015
Received in revised form 11 May 2016
Accepted 4 June 2016
Available online 6 June 2016

Keywords:
Trigger mechanism
Fjord
Mass transport
Holocene
Earthquake
Depositional environment

ABSTRACT

High resolution acoustic data and a 15.7 m long sediment core from the Hardangerfjorden system, western Norway, have been analyzed to increase our knowledge on depositional environments, submarine mass movement trigger mechanisms and submarine mass movement frequencies in high latitude fjord systems. The seismic profiles analyzed show that an up to 160 m thick glacimarine-dominated unit, of probably Younger Dryas age, has been deposited above the acoustic basement. A <55 m thick unit, comprising stacked mass transport deposits (MTDs) has been deposited atop the glacimarine unit. The identified mass movement events comprise 19 MTDs (MTD1–19), which have transported sediment volumes of up to 0.4 km^3 and initiated turbidity currents resulting in the deposition of up to 13 m thick turbidite layers. The established chronostratigraphical framework reveals high mass movement activity in Hardangerfjorden at 11100–8200 cal. yrs BP (Early Holocene) and at 4100 cal. yrs BP to present (Late Holocene). 14 MTDs have been dated to the Early Holocene, which is a time period characterized by high sedimentation rates (1.1 mm/yr), giving a mass movement recurrence rate of 1/200 years. Several of these failure events are suggested to have been triggered by regional mechanisms such as earthquakes linked to glacioisostatic uplift. Some of the MTDs of that time could potentially be caused by rock avalanches. Furthermore, it seems that the identified 8200 cal. yrs BP MTD5 coincides with the age of the Storegga tsunami, suggesting that processes related to this event may have caused sediment failure in the inner Hardangerfjorden. During the mid-Holocene (8200–4100 cal. yrs BP), a time period which was characterized by low sedimentation rates of 0.1–0.2 mm/yr and a warmer and wetter climate, mass movement events were absent in the study area. The renewed slide activity in the Late Holocene, comprising four MTDs, is probably related to climatic processes, earthquakes and rock avalanches, resulting in a mass movement recurrence rate of 1/1000 years for this time period. This study, thus, underlines the importance of high-latitude fjords, also in a global context, as systems where local, regional and external geological forces interact to impose highly dynamic postglacial depositional environments.

1. Introduction

Fjords are important source-to-sink systems at high latitudes on both the northern and southern hemisphere. These glacially-carved features, furthermore, represent the transition from the terrestrial to the marine environment, commonly comprising high resolution sediment archives recording climatic and environmental changes through time (Howe et al., 2010).

Mass movements, initiated subaerially, in shallow water depths or in the fjord seabed, are a frequently occurring sedimentary process within fjord systems and have been reported to occur worldwide (Syvitski et al., 1987), including a broad variety of different types as rock and snow avalanches, submarine slides, turbidity currents, slope creeping and cyclic steps. Their trigger mechanisms have, among others, been related to tectonic and climatic processes, increased pore pressures and human activity (e.g. Blikra et al., 2006; Hughes Clarke et al., 2014; Van Daele et al., 2013; Forwick and Vorren, 2007).

Mass movements within fjords may initiate tsunami waves (Haeussler et al., 2014), which can have a devastating effect on both coastline infrastructure and society (L'Heureux et al., 2010). The largest natural disasters in the 20th century in Norway, in Tafjord and Loen, were related to mass movements and following tsunamis (Blikra et al., 2006). With this background it is important to understand the trigger mechanisms and also the frequencies of such events in fjord regions. A number of studies describe mass transport deposits in fjords, but identification of trigger mechanisms have to a large extend been hampered as the chronostratigraphical constrains of mass movement events

* Corresponding author.
E-mail addresses: benjamin.bellwald@uib.no (B. Bellwald), berit.hjelstuen@uib.no (B.O. Hjelstuen), hans.sejrup@uib.no (H.P. Sejrup), haflidi.haflidason@uib.no (H. Haflidason).

http://dx.doi.org/10.1016/j.margeo.2016.06.002

mainly have relayed on 2–4 m long sediment cores, only giving information on very recent mass movement episodes (e.g. Lysså et al., 2009; Hjelstuen and Brendryen, 2014).

In this study we analyze a 15.7 m long Calypso core, high-resolution TOPAS seismic profiles and high-resolution bathymetric data from the third longest fjord in the world, the Hardangerfjorden system on the west coast of Norway (Fig. 1). The study aims to better understand mass movement trigger mechanisms and mass movement frequencies within a fjord system since the Last Glacial Maximum. This overall objective will be addressed through our study by the (1) establishment of a seismostratigraphical framework, (2) mapping and analyses of seismic facies and seabed features, (3) establishment of a precise chronology of the investigated sediments, (4) identification of different types of mass movements, and (5) relating the identified mass movements to the existing knowledge on Holocene climate development, colluvial systems, postglacial uplift history, and seismicity in the region. Finally, we discuss the global relevance of the Hardangerfjorden high-latitude fjord system regarding relationships between mass failures, sedimentation rates, seismicity and tsunami run-up.

2. Regional setting and geological background

This study focuses on the 160 km-long Hardangerfjorden system, of which the inner 65 km of the fjord, comprising Samlafjorden, Utnefjorden and Eidfjorden, represents the main area of interest (Figs. 1, 2). Hardangerfjorden is located in western Norway, about 40 km southeast of Bergen, and is surrounded by up to 1650 m high mountains and several tributary fjords. The up to 10 km wide fjord system cuts deeply into Precambrian rocks and follows a NE-SW trending shear zone, which shows no neotectonic activity (Fig. 1). However, in spite of this, the Hardangerfjorden region has a high seismicity compared to most other areas in Norway, and in the year of 2000 a M4.5 earthquake took place nearby the fjord mouth (Fig. 1b, Hicks and Ottemöller, 2001). We note that the estimated recurrence intervals for M5 and M7 earthquakes in Norway are 10 and 1100 years, respectively (Bungum et al., 2005).

The deepest part of Hardangerfjorden, with a water depth of 860 m, is reached in Samlafjorden (Fig. 2). Samlafjorden is bounded in southwest by a sill at Jondal (Figs. 1b, 2a), whereas Granvinsfjorden, a tributary fjord to the main Hardangerfjorden system, separates Samlafjorden from the 5 km long Utnefjorden (Fig. 2c). Utnefjorden has an E-W trend and its water depth shallows from 750 m in the northeast to 710 m where the fjord separates into Eidfjorden and Sørfjorden (Fig. 2b). Eidfjorden is a narrow fjord with steep fjord flanks (Figs. 1c, 2b), where the water depth decreases to 250 m near the fjord head. The steep fjord sides leave very little space for habitation, with Eidfjord at the head of the fjord as the biggest population center in this area of the Hardangerfjorden system (Fig. 2c). The study area hosts a

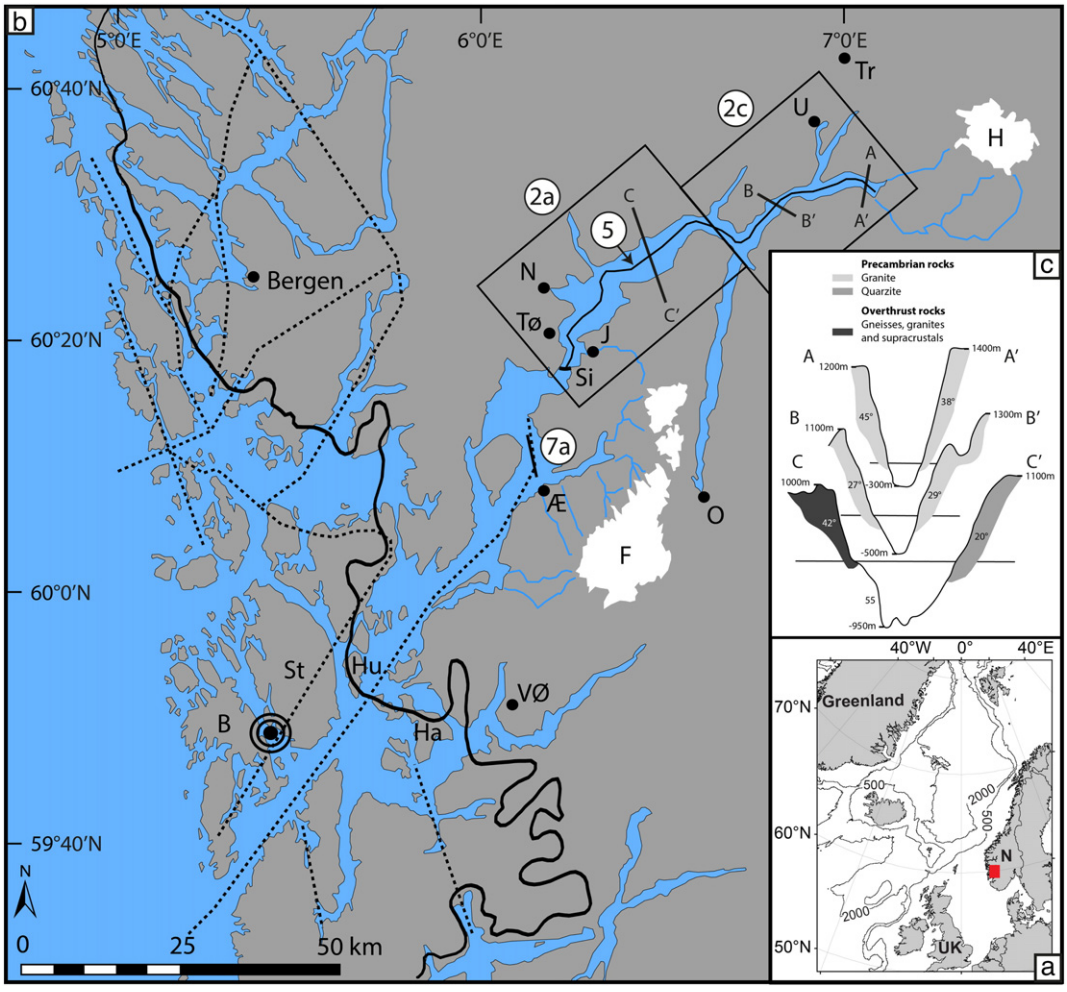

Fig. 1. (a) Regional overview map of the northern North Atlantic. Location of study area in red box. (b) Hardangerfjorden system. Significant faults systems (stippled lines), western extend of ice sheet during the Younger Dryas time period (black line), present glaciers (white areas) and epicenter of the M4.5 Stord/Bømlo earthquake in 2000 (black circles) are shown. Numbers given in white colored circles refer to figure numbers. Positions of slope profiles in c are shown. B: Bømlo, F: Folgefonna Glacier, H: Hardangerjøkulen Glacier, Ha: Halsenøy, Hu: Huglo, J: Jondal, N: Norheimsund, O: Odda, Si: Fjord-separating sill, St: Stord, Tr: Trettetjørn, Tø: Tørvikbygd, U: Ulvik, VØ: Vestre Øykjamyrtjørn, and Æ: Delta River Ænes. (c) Profiles across the Inner Hardangerfjorden showing variation in fjord morphology. Black horizontal lines indicate sea level. Profile locations in b.
Figure is modified after Holtedahl (1975).

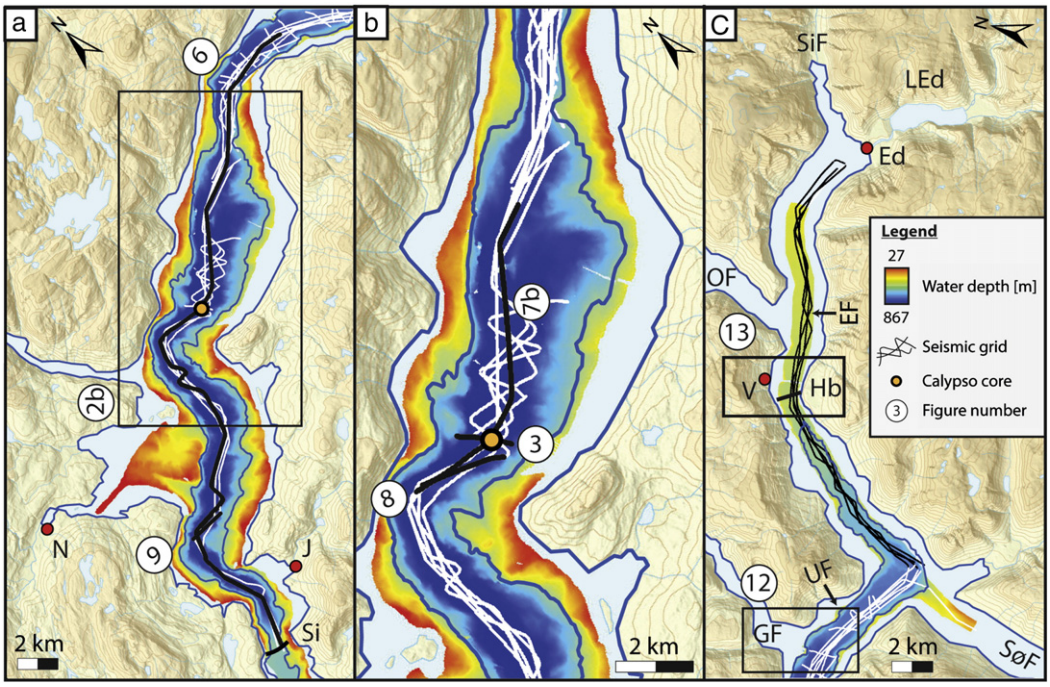

Fig. 2. Study area, (a) Samlafjorden, (b) Inner Samlafjorden, (c) Utnefjorden and Eidfjorden, with location of TOPAS seismic profiles (black and white lines), bathymetric records and sediment core analyzed. Numbers given in white colored circles refer to figure numbers. Ed: Eidfjord, EF: Eidfjorden, GF: Granvinsfjorden, Hb: Hardanger Bridge, J: Jondal, LEd: Lake Eidfjord, N: Norheimsund, OF: Osafjorden, SaF: Samlafjorden, Si: Fjord-separating sill, SiF: Simafjorden, SøF: Sørfjorden, UF: Utnefjorden, and V: Vangsbygdi.
Topographic information from www.geonorge.no.

population of ~23,000 inhabitants (www.ssb.no), and attracts many tourists in summer. Roads and power lines are following the fjord coastline, and the Hardanger Bridge is crossing Eidfjorden nearby Vangsbygdi (Fig. 2c).

The Hardangerfjorden system was completely covered by the Fennoscandian Ice Sheet during the Last Glacial Maximum and ice also filled the fjord-basin as far southwest as the Huglo and Halsnøy islands during the 12.8–11.6 cal. kyrs BP Younger Dryas Stadial (Mangerud et al., 2013, Fig. 1b). During this stadial the ice sheet exceeded 2000 m in thickness, and possibly grounded on shallow bedrock sills. The Younger Dryas time period ended with the final retreat of the Fennoscandian Ice Sheet. The ice sheet withdrew faster from the Hardangerfjorden system (240 m/yr) than the melting of the ice on land, and in only 500 ± 140 years the ice sheet had reached the head of the fjord (Mangerud et al., 2013). Today, the catchment area of Hardangerfjorden is still partly glaciated by the Folgefonna and Hardangerjøkulen ice caps (Fig. 1b), and the rivers originating from these ice caps have higher sediment discharge than rivers draining non-glaciated areas (www.nve.no). These two ice caps did not exist in the mid-Holocene (Bakke et al., 2005; Dahl and Nesje, 1996). It should also be noted that lakes located close to the head of the fjord, such as Lake Eidfjord, and tributary fjord basins, such as Granvinsfjorden (Fig. 2b), may act as sediment traps, and decrease the sediment supply into the main fjord system. At present, pelagic sediments accumulate with rates of <1 mm/yr in western Norwegian fjords (Aarseth et al., 1989).

The identified sediment basins in Hardangerfjorden are mainly filled with fine-grained postglacial sediments that reach a maximum thickness of 240 m, corresponding to a sediment volume of about 19 km^3, of which 3 km^3 are belonging to the study area of this work (Aarseth, 1997).

Shallow gravity cores have shown that the fine grained sediments in the uppermost two meters of the fjord basin infill are interrupted by several thin coarse-grained layers, which are related to turbidity currents (Holtedahl, 1975). Only one of these turbidite layers has been dated, showing that turbidity currents were active in the Hardangerfjorden system at about 5250 ± 150 ^{14}C years BP (5608 ± 35 cal. yrs BP). A study by Bøe et al. (2004), which combines information from a number of fjords in western Norway, concludes that turbidity currents seem to dominantly have occurred around specific time periods, i.e. at 8200, 2800 and 2100 cal. yrs BP.

Recent studies from Eidfjorden (Fig. 2c) have, furthermore, revealed that mass failures have been triggered in the basin plain of this fjord, giving rise to impressive slide scars. Bellwald et al. (2016) suggest that there is a relation between the location of these slide scars and the sediment supply into the fjord system by fluvial and colluvial processes.

3. Data and methods

The present study is based on high-resolution bathymetric data, high-resolution TOPAS seismic profiles and a 15.7 m long Calypso core (Figs. 2, 3). The bathymetric data sets have been collected by the University of Bergen (UiB) and DOF Subsea AS. The UiB data set (Fig. 2) was collected onboard R/V G.O. Sars in 2004 using a hull mounted EM1002 (95 Hz) system. These data have been processed and gridded with a cell size of 25 × 25 m utilizing the Neptun and Fledermaus softwares. The bathymetric records from DOF Subsea AS was acquired in 2010 with a Kongsberg EM710 MBE system (70–100 kHz) and a ROV mounted Seabat 7125 (200 and 400 kHz). These records were gridded with a cell size of 1 × 1 m and 0.2 × 0.2 m, respectively.

A total of ~400 km of sub-bottom profiles (TOPAS PS18, 0.5–6 kHz) was collected during UiB cruises onboard R/V G.O. Sars in 2005 and 2014 (Fig. 2). In general, the quality of these seismic profiles, which have a vertical resolution of ~30 cm, is good. The seismic data were interpreted based on changes in seismic facies, using the Petrel software (v.2013) from Schlumberger AS. Based on results from Multi-Sensor Core Logging (MSCL) of the acquired Calypso core, sediment velocities of 1500 m/s have been applied in order to estimate sediment thicknesses and sediment volumes of the identified seismic units.

The 15.7 m long Calypso core (GS14-187-03PC, 60° 23.190′N/ 6° 22.201′E) was retrieved from a water depth of 857 m in Samlafjorden

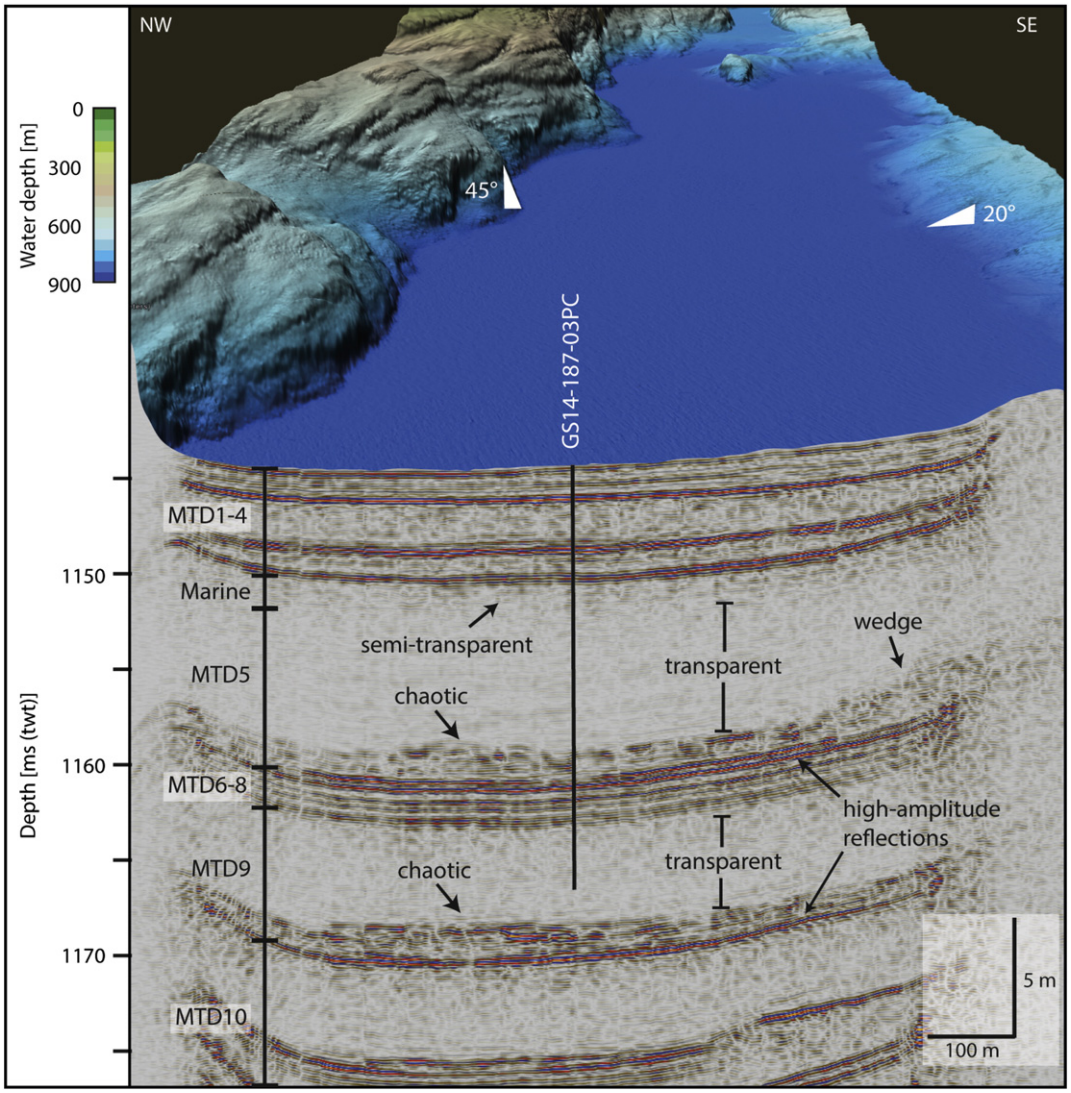

Fig. 3. Bathymetric and sub-bottom setting of core GS14-187-03PC. Bathymetry in 3D view. Bathymetry from DOF Subsea Norway and Statnett.

(Figs. 2b, 3), and analyzed at the Department of Earth Science, UiB. Using a Geotek MSCL 7.9, bulk density, magnetic susceptibility and P-wave velocities were measured every 0.2 cm down the core prior to the splitting of the core sections. After splitting, the core segments were X-radiographically scanned by an Itrax Core Scanner (COX Analytic Systems), before the core sections were visually described and the sediment color was determined by a Munsell Soil Color Chart. Undrained shear strength was measured every 5 cm using a standard fall cone test (Hansbo, 1957) with cone weights of 60 g, 100 g and 400 g. In total 321 fall cone measurements were taken.

Table 1
Radiocarbon dates Calypso core GS14-187-03PC.

Laboratory code	Depth [cm]	Uncalibrated age [yrs BP]	±1σ	Calibrated age [yrs BP]	Standard deviation	Material	Weight [mg]
ETH-59432	5–8	1660	36	1216	76	Foraminifera	3.2
ETH-60797	8–11	2058	30	1624	90	Foraminifera	2.6
ETH-59433	37–44	3049	49	2833	108	Foraminifera	1.9
ETH-60798	294–300	3776	30	3717	103	Foraminifera	3.9
ETH-59434	337–340	4195	54	4271	156	Foraminifera	2.5
ETH-59435	371–373	5909	50	6324	109	Foraminifera	3.4
ETH-59436	411–414	7362	53	7815	119	Foraminifera	2.9
ETH-60799	414–420	7375	30	7840	84	Foraminifera	7.4
ETH-59437	967–976	8905	47	9573	111	Foraminifera	7.3
ETH-59438	982–988	8548	56	9184	169	Foraminifera	4.0
ETH-59439	1057–1066	9149	60	9916	217	Foraminifera	4.4
ETH-59440	1112–1115	10,628	63	11,957	319	Foraminifera	3.9
ETH-60800	1131–1137	9621	36	10,506	116	Foraminifera	5.0
ETH-59441	1161–1164	9738	54	10,652	155	Marine shells	5.4

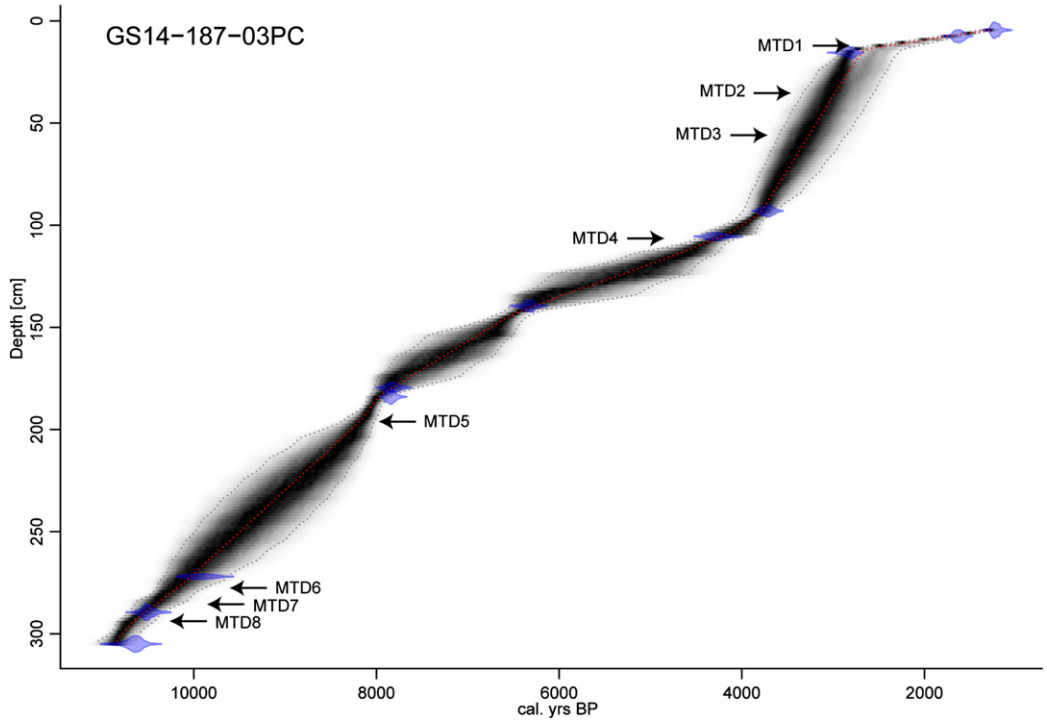

Fig. 4. Age model of core GS14-187-03PC utilizing the Bacon software. Note that depth excludes MTDs. Level of MTD and ^{14}C AMS datings (blue lenses) are indicated.

The core was then sub-sampled in intervals of 10 cm for water content, grain size analysis and accelerator mass spectrometry (AMS) ^{14}C dating. A total of 180 samples were extracted from the core and wet sieved for the ≥63 μm, ≥125 μm and ≥250 μm grain fractions. Fourteen samples of the grain size fraction ≥ 125 μm were picked for benthic foraminifera species (*Pyrgo* sp., *Uvigerina* sp., *Hyalinea balthica*, *Elphidium excavatum*), ostracods or marine shells for the AMS ^{14}C dating. Depending on sample weight, the sample intervals varied between 3 and 9 cm. The radiocarbon levels for dating were chosen in order to get a best possible chronostratigraphy for the core and for the identified mass transport deposits. The AMS radiocarbon dating analyses were performed at ETH Zürich, and afterwards calibrated using OxCal v4.2.4 (Bronk Ramsey, 2013) and Marine13 marine curve (Reimer et al., 2013) with the standard reservoir correction of 405 ^{14}C years and a $\Delta R = 0$. The calibrated ages are presented as ages before present (cal. yrs BP, where present is 1950 CE) within the 1σ range (Table 1). In addition, an age

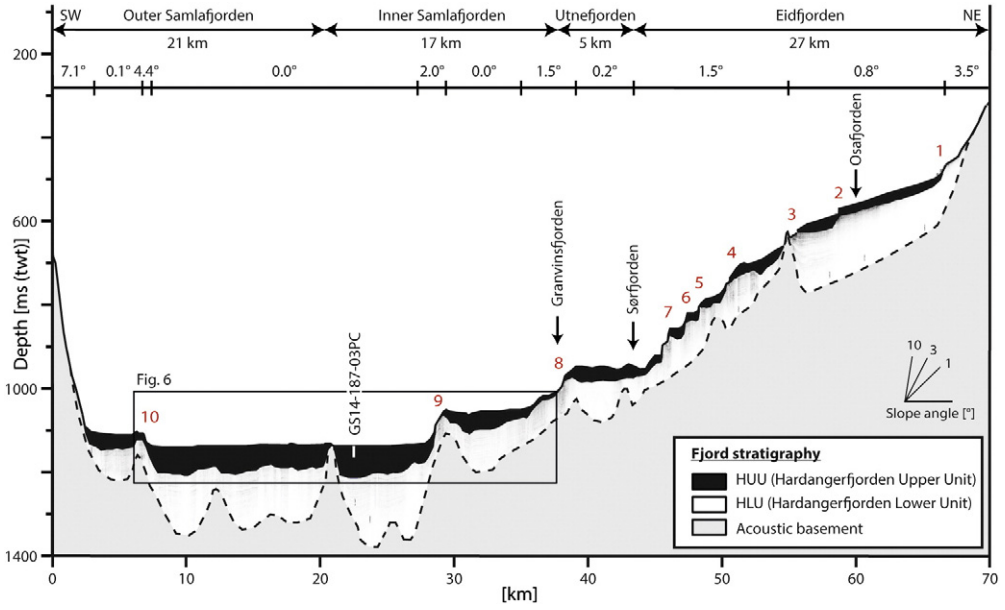

Fig. 5. Geoseismic profile from the inner Hardangerfjorden system. Profile location in Fig. 1b. Fjord basins, tributary fjords (black arrows), fjord stratigraphy, coring location, slide scars (red numbers) and gradient of the fjord bottom are indicated.

model of the background sedimentation has been created with the Bacon v.2.2 software (Blaaw and Christen, 2011), in which identified mass transport deposits have been excluded (Fig. 4).

4. Results

4.1. Seismic stratigraphy and seismic facies

The interpretation of the ~400 km of sub-bottom profiles show that the acoustic basement in the study area is represented by unsystematic low-amplitude reflections, defining a highly irregular surface which locally almost reaches the surface of the seabed (Figs. 5, 6, 13d) and separates the fjord into several sub-basins. Above the acoustic basement, the Inner Hardangerfjorden is filled by up to 210 ms(twt) (158 m) of sediments, representing an estimated sediment volume of ~3 km^3 (Fig. 5). The sediment package, which partly smooths out the irregular surface of the acoustic basement, is thickest in the deepest part of the fjord system whereas it is reduced in thicknesses towards the fjord sides and shallower water (Fig. 5). The sediment package can be divided into two seismic units, which we name the Hardangerfjorden Lower Unit (HLU) and the Hardangerfjorden Upper Unit (HUU) (Figs. 5–7, 13).

The stratigraphically lower unit, HLU, consists of parallel, continuous, high-amplitude reflections that are intercalated by 50 less than 2 m thick acoustically transparent layers (Figs. 6, 7b, 13d). HLU comprises a maximum sediment thickness of 140 ms(twt) (105 m) in both Samlafjorden and Eidfjorden (Fig. 5). We interpret HLU, characterized by continuous reflections within all basins, as glacimarine deposits (Figs. 6, 7). This interpretation is supported by studies from Fensfjorden (Hjelstuen et al., 2013) and Byfjorden (Hjelstuen and Brendryen, 2014), north of our study site. Even though the Calypso core does not penetrate into this unit, we suggest the same sediment composition of the HLU as HUU when similar seismic facies are identified.

The upper identified seismic unit, HUU, varies in maximal thickness from 70 ms(twt) (53 m) in Samlafjorden to 20 ms(twt) (15 m) in Eidfjorden (Figs. 5, 6), and is characterized by three different acoustic facies; chaotic, transparent and parallel (Figs. 3, 7, 8). The acoustically chaotic facies is characterized by discontinuous moderate to high amplitude reflections, defining either regionally or locally identified wedges with a maximal thickness of up to 10 m (Figs. 6–9). The wedge geometry is best-identified close to 10 identified vertical steps, suggested to represent slide scars (Bellwald et al., 2016), and the fjord flanks, from where they are then pinching out into more distal areas (Figs. 6, 7). The chaotic packages are further characterized by overthrusting and are either overlying a high-amplitude reflection or locally cutting into the underlying sediments (Fig. 8). We note that close to the Hardanger Bridge, this chaotic facies show a lensoid shape, comprising a volume of ~$30 \cdot 10^6$ m^3 (Fig. 13d), which we suggest to represent a rock avalanche deposit. This is supported by a study of Lysså et al. (2009) in Nordfjord, who came to the same conclusion for a comparable seismic package.

The acoustically transparent facies (Figs. 3, 7) is covering areas of up to 30 km^2, comprises volumes of up to 0.4 km^3 and can be traced for distances of ~40 km. We term the identified acoustically transparent facies, locally underlain by acoustically chaotic facies, as Mass Transport

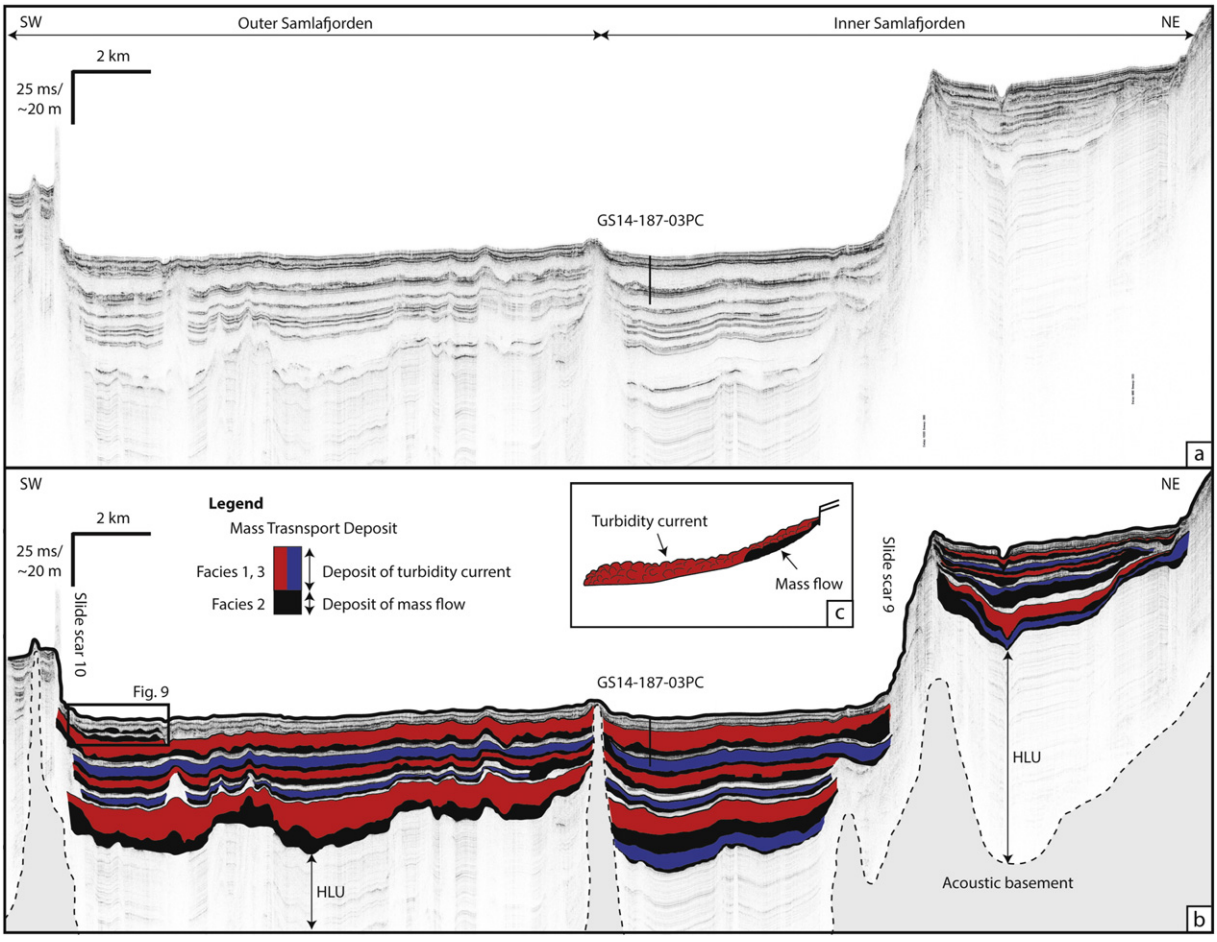

Fig. 6. (a) Seismic profile from Samlafjorden. Profile location in Fig. 5. (b) Interpretation of seismic profile from Samlafjorden showing the character of the Hardangerfjorden Lower Unit (HLU) and Hardangerfjorden Upper Unit (HUU). (c) Schematic model of suggested mass wasting process.

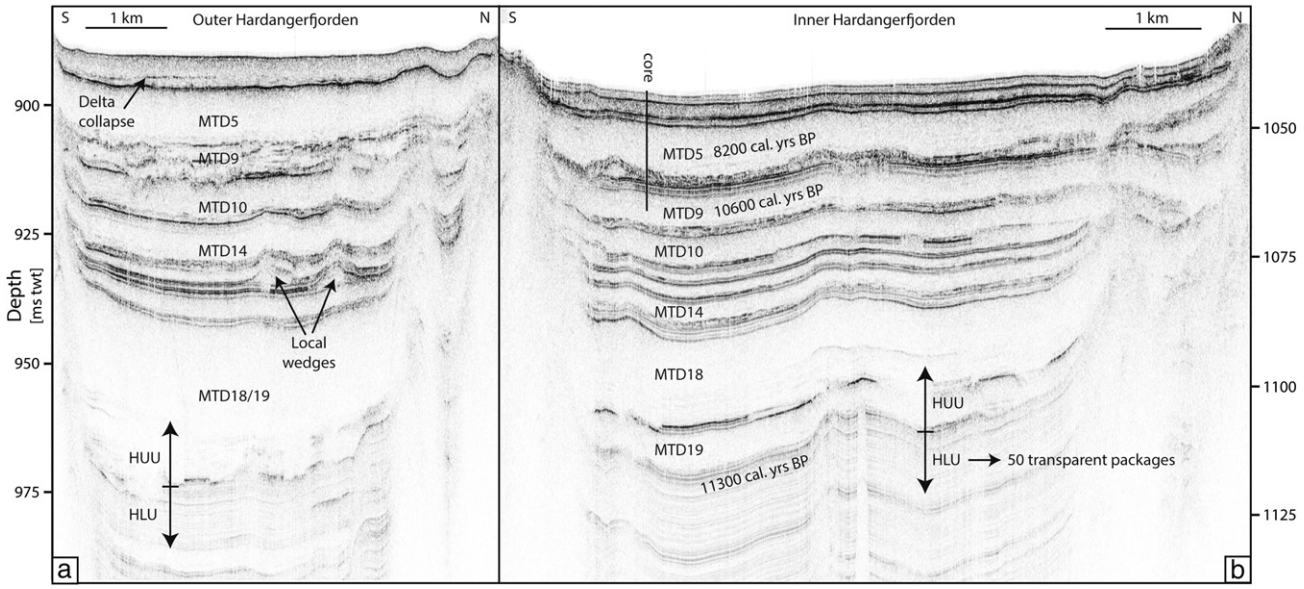

Fig. 7. Seismic character of the two main identified seismic units, Hardangerfjorden Upper Unit (HUU) and Hardangerfjorden Lower Unit (HLU), and correlation of MTDs in the (a) Outer and (b) Inner Hardangerfjorden. Core is projected position of GS14-187-03PC. For profile locations, see Figs. 1 and 2.

Deposits (MTDs), following the terminology as is established in Canadian fjords by St-Onge et al. (2012). A total of 19 MTDs have been identified in the HUU (MTD1 (youngest) – MTD19, Figs. 6, 7; Table 2).

Some of the identified MTDs are characterized by meter-sized acoustically transparent facies, varying in thickness between 2 and 15 m. These meter-sized MTDs are always overlying acoustically chaotic

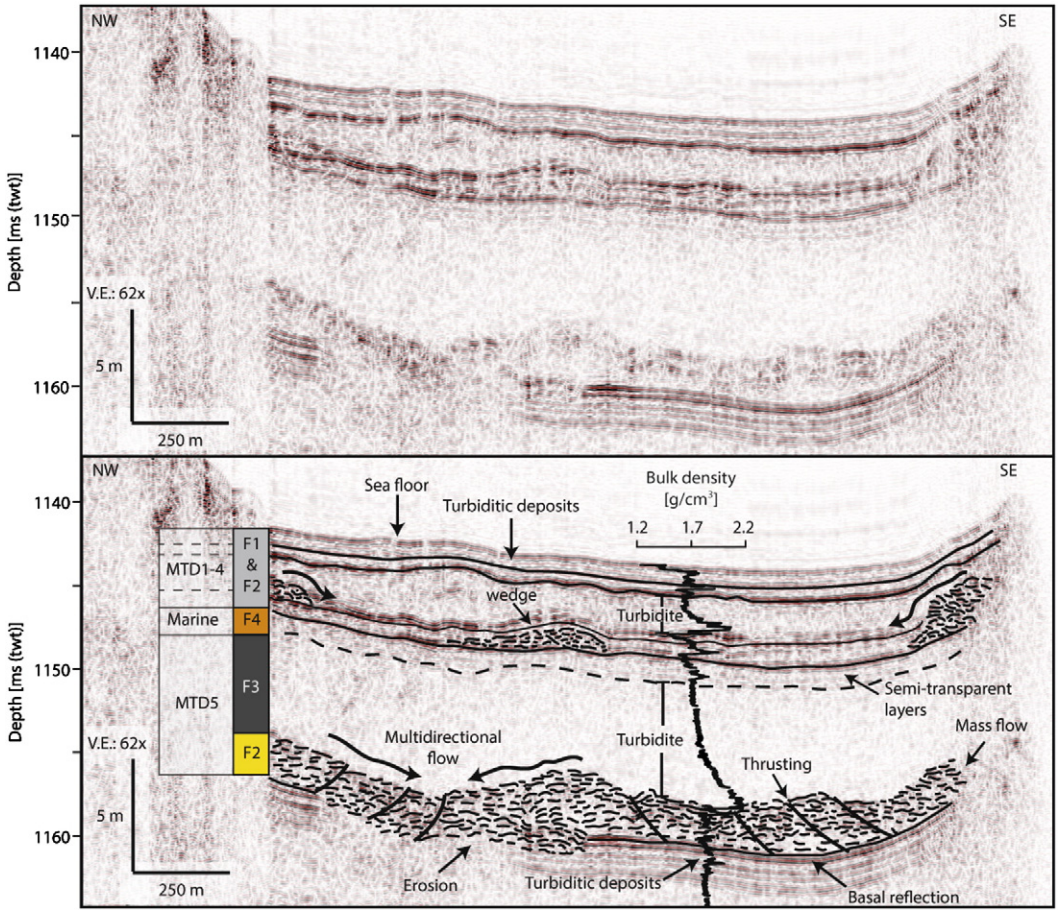

Fig. 8. Upper panel: Seismic example of the uppermost part of the identified HUU seismic unit. Lower panel: Interpretation of seismic example. MTD5 indicates basin-wide, bi-directional mass flow (black arrows) and thrusting (black lines) of mass flow deposits, whereas multiple local wedges have been identified for MTD4, one wedge for MTD3, and no wedges for MTD1 and MTD2 in this profile. Bulk density values shown are from the analyzed Calypso core. V.E.: Vertical exaggeration. Figure location in Fig. 2b.

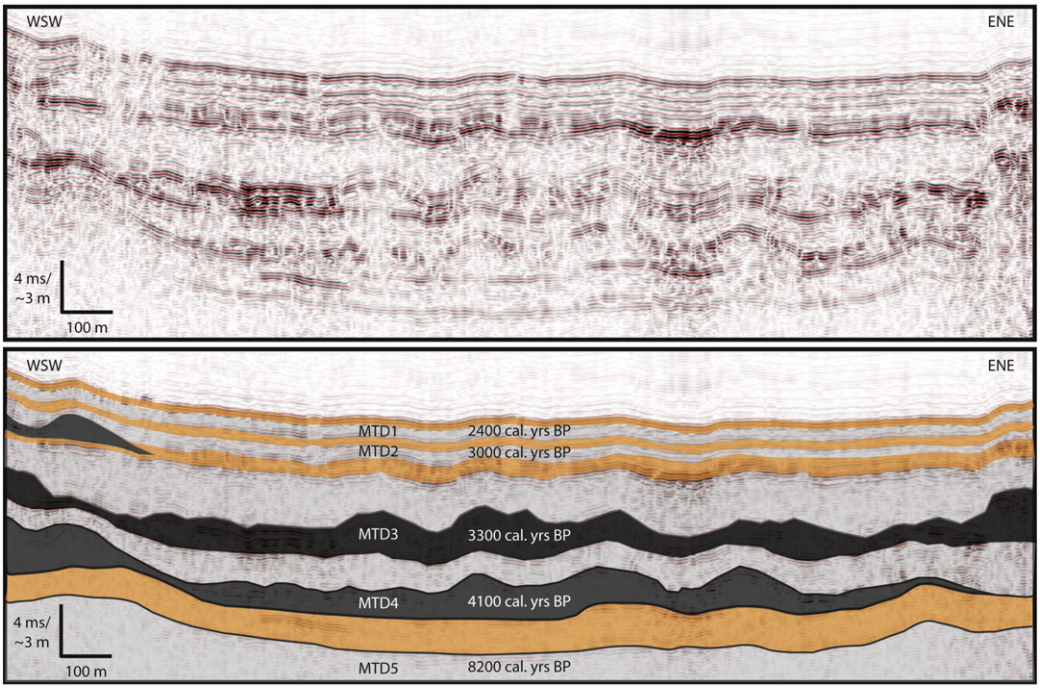

Fig. 9. Upper panel: Seismic example from southwestern part of Samlafjorden showing characteristics of suggested locally triggered mass transport deposits (MTD1–4). Lower panel: Interpretation of seismic line shown in upper panel. Marine deposits (orange), turbiditic deposits (gray) and mass flow deposits (dark gray) are indicated. The seismic reflections have been traced from the core location to the seismic profile. Location of profile in Fig. 2a.

facies. We term MTDs characterized by 0.2 to 2 m thick acoustically transparent packages and which only are overlying acoustically chaotic reflections locally (Figs. 8, 9) as decimeter-sized MTDs. We note that the identified MTDs also commonly are separated by acoustically (semi-)parallel reflections. Based on an average depositional area of about 30 km^2, the individual MTD volumes have been calculated to range between $4 \cdot 10^6$ m^3 and $383 \cdot 10^6$ m^3 (Table 2).

4.2. Lithostratigraphy

The analysis results of the 15.7 m-long Calypso core (Fig. 10) suggests that the fjord sediments in this part of Hardangerfjorden can be separated into four lithological facies, Facies 1 to 4. Facies 1 and 3 are further subdivided into sub-facies 1a/1b and 3a/3b (Table 3). Sub-facies 1a is dominated by fine-grained mud, an absence of sand and low variance in its geophysical and geotechnical properties. The sub-facies is further characterized by low shear strength and high water content. Sub-facies 1b, which stratigraphically always underlies Sub-facies 1a, is characterized by normal grading from fine mud to fine sand with an increase of sand content to a value of up to 9% towards the base. Density, magnetic susceptibility and shear strength values are also increasing downwards. Sedimentary structures such as fine sandy layers and erosive flow behavior are observed at the base of the Sub-facies 1b (Fig. 11a).

Table 2
Dimensions, suggested ages and suggested trigger mechanisms of the identified MTDs. Note that the age of MTD10–19 have been estimated based on the seismostratigraphy and suggested sedimentation rates.

MTD	Thickness [ms]	Thickness [m]	Volume [km^3]	Volume [10^6 m^3]	Suggested age [cal. yrs BP]	Trigger mechanism	Suggested trigger mechanism
1	0.50	0.23	0.007	7	2400	Regional	Earthquake
2	0.50	0.34	0.010	10	3000	Local/regional	Rock avalanche/earthquake
3	2.75	1.45	0.044	44	3300	Regional	Earthquake
4	0.50	0.29	0.009	9	4100	Regional	Earthquake
5	9.00	5.79	0.174	174	8200	Regional	Earthquake/tsunami
6	0.50	0.35	0.011	11	10,200	Local/regional	Rock avalanche/earthquake
7	0.25	0.20	0.006	6	10,400	Local/regional	Rock avalanche/earthquake
8	0.25	0.13	0.004	4	10,600	Local/regional	Rock avalanche/earthquake
9	7.25	5.44	0.163	163	10,700	Regional	Earthquake
10	8.25	6.19	0.186	186	10,700–11,100	Regional	Earthquake
11	0.50	0.38	0.011	11		Local/regional	Rock avalanche/earthquake
12	2.50	1.88	0.056	56		Local/regional	Rock avalanche/earthquake
13	0.25	0.19	0.006	6		Local/regional	Rock avalanche/earthquake
14	4.75	3.56	0.107	107		Regional	Earthquake
15	0.50	0.38	0.011	11		Regional/local	Earthquake/rock avalanche
16	0.75	0.56	0.017	17		Regional/local	Earthquake/rock avalanche
17	0.50	0.38	0.011	11		Regional/local	Earthquake/rock avalanche
18	17.00	12.75	0.383	383		Regional	Earthquake
19	8.00	6.00	0.180	180		Regional	Earthquake
Total			1394	1394			

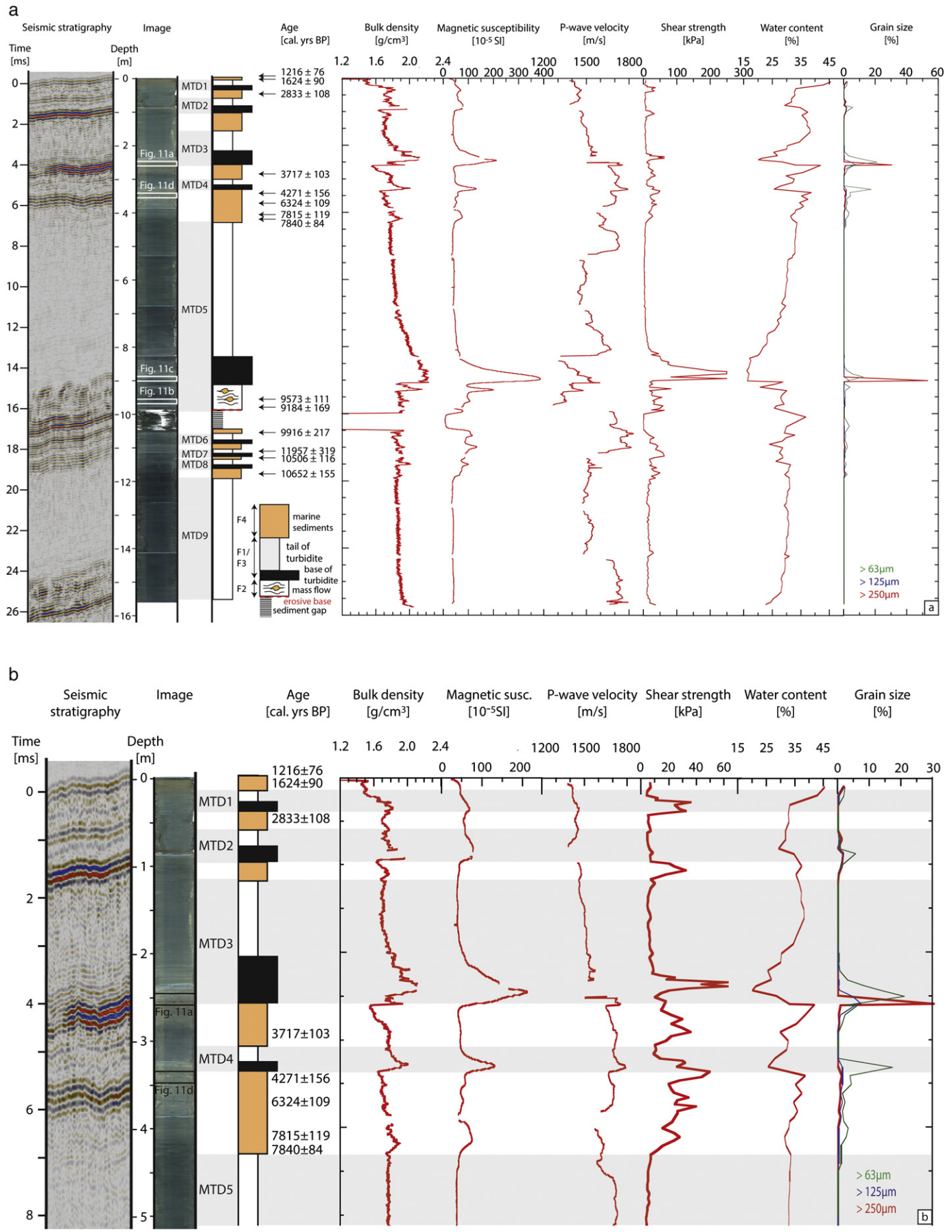

Fig. 10. (a) Geophysical, geotechnical and sedimentary results of analyzed Calypso core GS14-187-03PC. Identified MTDs, correlation to seismic profile and $_{14}$C dates are also shown. (b) Blow-up of uppermost 5 m of Calypso core. Legend as in a.

Table 3
Characteristics of identified litho-facies 1–4.

Criteria	Facies 1a	Facies 1b	Facies 2	Facies 3a	Facies 3b	Facies 4
Seismical						
Reflection geometry	Transparent Discontinuous	Parallel Continuous	Chaotic Discontinuous	Transparent Discontinuous	Transparent Discontinuous	Parallel Semi-continuous
Reflection continuity	Low to moderate	Low to moderate	Moderate to high	Low to moderate	Low to moderate	Moderate
Amplitude						
Thickness [m]	<1	<0.5	<10	1–15	<1	<1
Geometry	Draping	Draping	Wedging-pinching out	Ponding-draping	Ponding-draping	Draping
Geophysical						
Bulk density [g/cm^3]	1.4–1.8	1.5–2.0	1.9–2.2	1.7–2.0	2.0–2.2	1.6–1.9
Magnetic susceptibility [10^{-5} SI]	40–60	50–140	50–200	40–50	50–400	50–75
P-wave velocity [m/s]	1400–1700	1400–1700	1300–1500	1450–1750	1500–1700	1400–1700
Geotechnical						
Shear strength [kPa]	7–10	10–56	18–83	10–20	20–250	8–40
Sedimentological						
Sand content [%]	0	0–9	0–18	0	0–59	0–6
Water content [%]	30–40	25–35	21–37	23–35	16–23	31–45
Visual						
Structures	Homogenous clay	Fining-upwards from fine sand into clay, sandy interlayers, erosive base	Deformations, sand accumulations, clasts, grain sorting, erosive base	Homogenous clay	Fining-upwards from coarse sand into clay, sandy interlayers, erosive base	Shell remnants, bioturbation, gas cracks, laminations
Color	Very dark gray	Very dark gray	Very dark gray	Very dark gray Black	Greenish black	Very dark greenish gray
Interpretation						
Process	Tail of turbidite	Base of turbidite	Mass flow	Tail of megaturbidite	Base of megaturbidite	Marine

Likewise to Facies 1, Facies 2 is characterized by fine-grained mud, but with sand layers distributed throughout the facies. Facies 2 has a high density, moderate shear strength and low water content. Deformation structures, dominated by contorted sediment, are observed (Fig. 11b). The fine-grained mud that defines Sub-facies 3a has similar visual and sedimentological as Sub-facies 1a, but has slightly higher density and shear strength values. Sub-facies 3b shows normal grading from fine mud to coarse sand, where the sand content increases over ~1 m from 0% at the top to 59% to the base of the sub-facies. The base of the sub-facies shows extreme peaks in density, magnetic susceptibility and shear strength (Fig. 10). Similarly to Sub-facies 1b, erosive behavior is observed at the base of the Sub-facies 3b (Fig. 11c). Facies 4 (Table 3, Fig. 11d) consists of fine-grained mud with a sand content of up to 6%. The facies is not graded, has a moderate to low density, low shear strength and high water content. Shell remnants, bioturbation structures, stratified sediment and randomly distributed foraminifera have been observed in this facies.

The 14 radiocarbon datings from the core suggest that the sediments are of Younger Dryas and Holocene age (Table 1, Fig. 10). Utilizing the established age constrains, and after the identified MTDs have been subtracted, we estimate background sedimentation rates of 1.1 mm/yr for the time period of 10,600–10,500 cal. yrs BP and 0.1–0.2 mm/yr for the 10,500–4300 cal. yrs BP time period. An increase in sedimentation rate to 0.7–0.9 mm/yr is observed in the 4300–2800 cal. yrs BP time period, whereas the sedimentation rates decreased to 0.1 mm/yr in the 2800–1200 cal. yrs BP time period (Fig. 14). We note that no or very little overpenetration of the core is suggested if utilizing the same sedimentation rates as estimated for the 2800–1200 cal. yrs BP time period to the sediments deposited during the last 1200 years. Furthermore, the ages of the MTDs (Table 2) have been estimated based on the age model (MTD1–9) or based on seismostratigraphy and suggested sedimentation rates (MTD10–19).

4.3. Correlation of seismic and lithological facies

The acoustically transparent facies identified in HUU and which is showing ponding geometry correlates with the normally-graded Facies 1 and 3 in the sediment core (Fig. 10). The peaks in shear strength, density and magnetic susceptibility at the base of these lithological facies, the absence of foraminifera and the absence of bioturbation combined with erosive flow behavior are all indicators for them to represent the suspensive load of erosive turbidity flows. This interpretation correlates with the definitions given by Mulder and Cochonat (1996), who defined turbidity flows as gravity flows in a turbulent regime. We also note that the two youngest identified MTDs in this study, MTD1 and MTD2 (Figs. 9, 10), have been interpreted to be turbidite beds in short cores in previous studies by Holtedahl (1975).

The identified acoustically chaotic facies (Figs. 6, 7) are suggested to represent the cohesive mass flow deposits, defined as gravity flows in a laminar regime (Mulder and Cochonat, 1996). This is supported by local erosion into deeper strata (Fig. 8) as well as low water content and deformation structures caused by reworking processes as observed in the correlatable Facies 2 in the core (Figs. 10, 11b). The observed overthrusting structure of the acoustically chaotic facies (Fig. 8) is furthermore a typical kinematic indicator for the deposition domain of a mass flow (Schnellmann et al., 2005; Alfaro and Holz, 2014). Non-chronostratigraphically order of the datings in one of these chaotic package and strongly variable sand content (Fig. 10) further indicate sediment reworking.

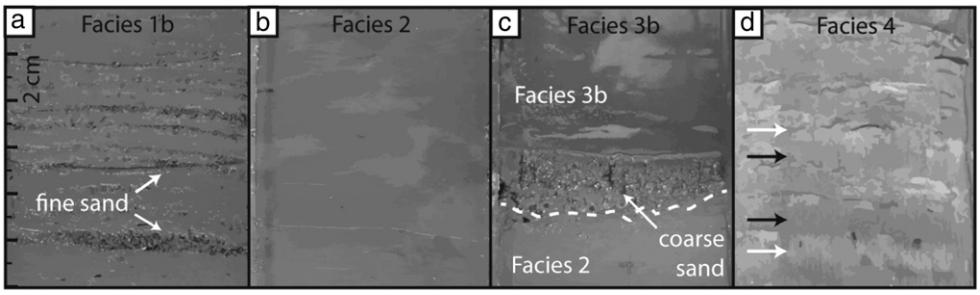

Fig. 11. X-ray images of identified litho-facies. Locations in Fig. 10. (a) Facies 1b is fine sandy layers at the base of homogenous mud (not shown), (b) Facies 2 is characterized by deformation structures in silty to clayey sediment, (c) Facies 3b is coarse sandy layers with an erosive base overlain by homogenous mud (not shown), (d) Facies 4 is characterized by laminated (arrows) and bioturbated sediment.

The identified acoustically semi-parallel reflections correlate to Facies 4 (Fig. 10). The low density, the low shear strength, the low water content, the randomly distributed foraminifera and the signs of bioturbation indicate that these sediment packages are representing marine deposits. Due to limitation in seismic resolution, Facies 4 cannot always be identified in the seismic data. We note that Facies 4 can be clearly distinguished from the MTDs (Facies 1–3) by their different color (very dark greenish gray), the presence of foraminifera and bioturbation as well as the absence of sediment reworking structures. Such diagnostic criteria have also been used by Sumner et al. (2013). The sand content of Facies 4, up to 6%, further allows us to clearly separate these acoustically semi-parallel reflections from the tails of the turbidites (sand content: 0%) as well as the base of the turbidites (sand content: up to 59%) or the acoustically chaotic facies at the bottom of the MTDs (sand content: up to 18%).

4.4. Seabed features

The estimated low background sedimentation rates in Hardangerfjorden allow for detection of seabed features in the bathymetric data, thus making it possible to relate the flat fjord bottom, the steep fjord flanks and the tributary fjords to the 19 MTDs, identified in the seismic profiles and the sediment core, and to make conclusions on present mass wasting processes.

The basin plain of the inner Hardangerfjorden is 400–3000 m wide and flanked by steep fjord sides, with average gradients of ~45° in the northwest and ~25° in the southeast (Figs. 3, 12, 13). The basin plain is flat to gently sloping in Samlafjorden, with some locations showing gradients of up to 4.4° (Fig. 5). The basin plain is cut by 10 slide scars, up to 35 m in height and 35° in inclination (Figs. 6, 12, 13), which are also observed in the seismic data. The slide scars are located in different

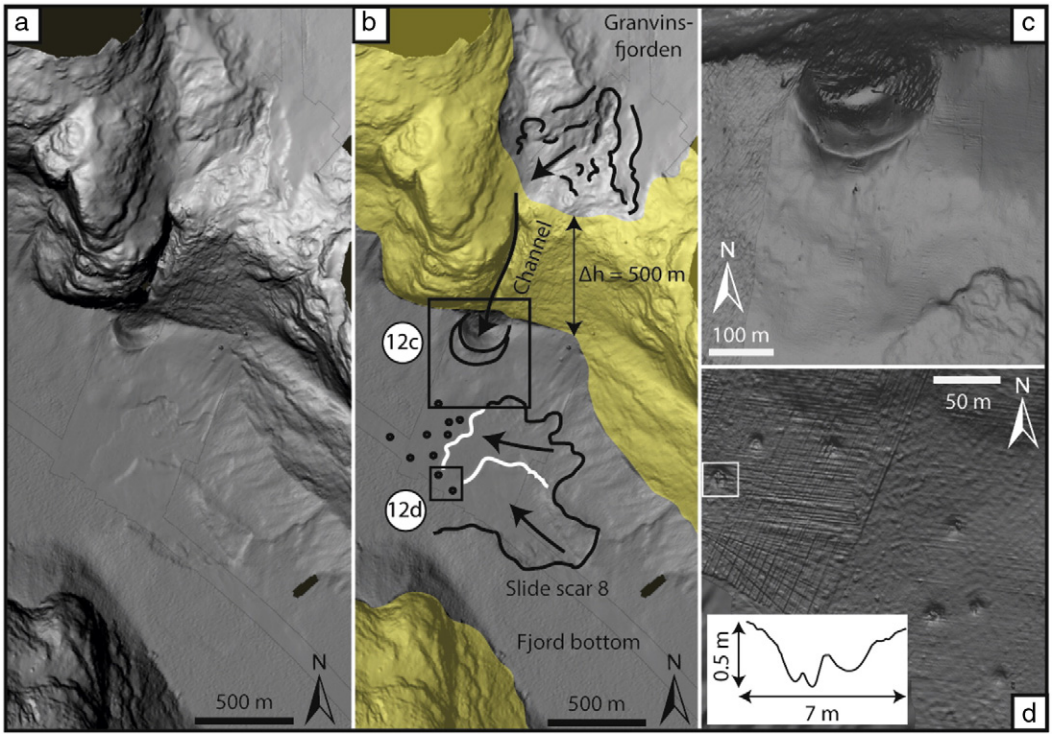

Fig. 12. Characteristic seabed features around slide scar 8. Location in Fig. 2c. Bathymetry from DOF Subsea Norway and Statnett. (a) Gray-shaded bathymetric overview image. (b) Interpretation of seabed-features in a. Fjord walls (yellow areas), slide scars (black lines), removed sediment blocks (white lines), sediment transport direction (black arrows) and pockmarks (black points) are indicated. (c) Crater-shaped feature (depth: 30 m, radius: 100 m) at the flat fjord basin flank and slide scar at fjord bottom. Figure location in a. (d) Blow-up of pockmark field with bathymetric profile through the pockmark shown in white box. Figure location in b.

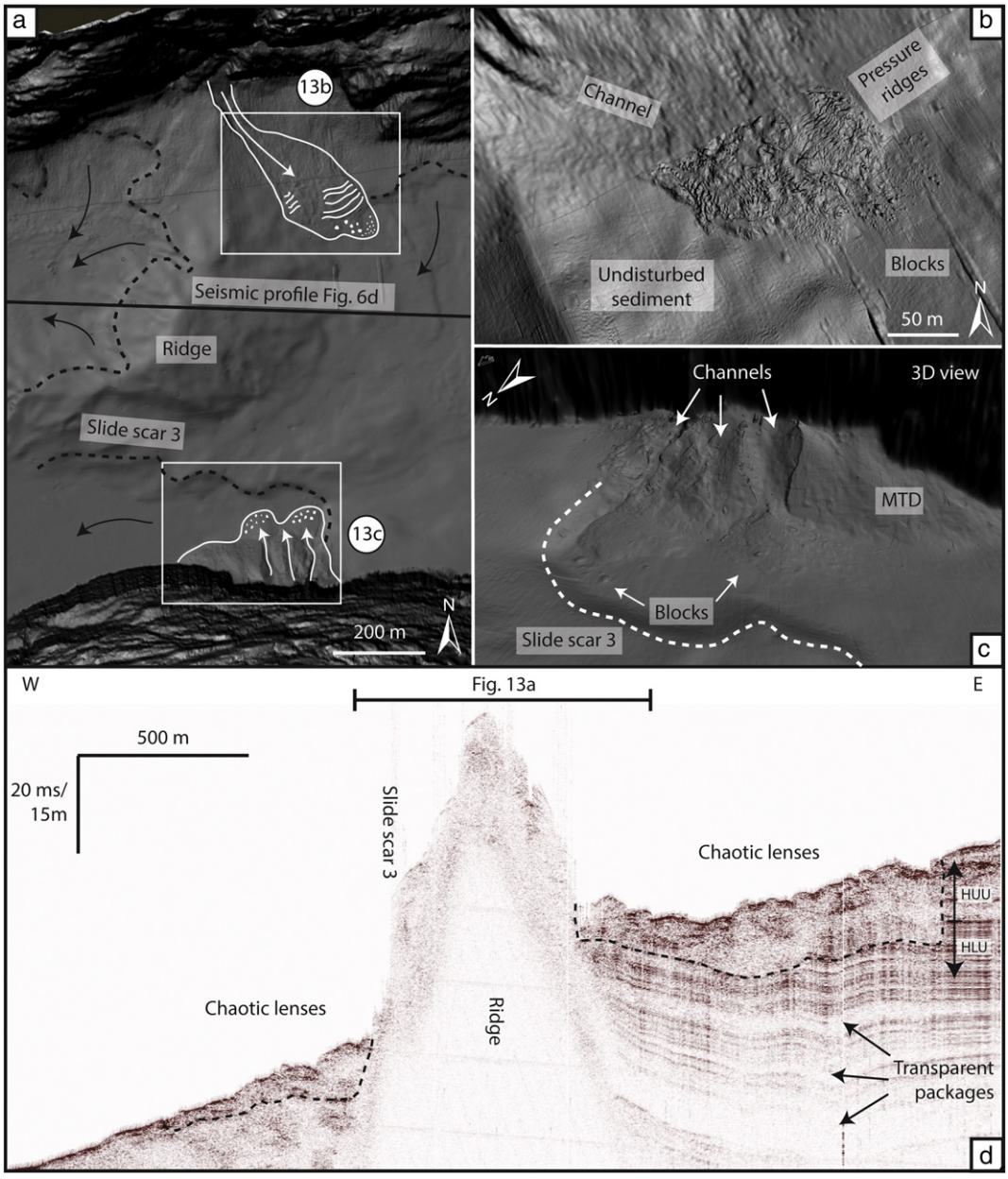

Fig. 13. Seabed imaginary of mass wasting at Vangsbygdi in Eidfjorden. Figure location in Fig. 2c. Bathymetry from DOF Subsea Norway and Statnett. (a) Fjord-crossing ridge, slide scars in the fjord bottom (black stippled lines), sediment transport directions (black arrows), mass wasting from fjord flanks (white arrows), extent of mass wasting (white line), pressure ridges (white short lines) and blocks (white points). (b) Pressure ridges and blocks in the contraction zone of the MTD. Location in a. (c) Mass wasting processes eroding into older MTDs. Figure location in a. (d) Seismic profile, location indicated in a, showing character of MTDs (lower limit indicated by black stippled lines). HLU: Hardangerfjorden Lower Unit and HUU: Hardangerfjorden Upper Unit.

fjord basins. They are commonly observed some kilometers in distance from each other, often in areas with steeper seafloor gradients. Most of the scars are found close to thresholds in the acoustic basement (Fig. 5). Such thresholds seem to have a controlling effect on surface slopes, exposing sediment to slope gradients of up to 4.4°. The slide scars cross the flat fjord bottom in water depths of 335–835 m and are commonly seen as sets of steps (Fig. 12b).

Up to 50 circular concave, crater-like depressions, ~4 m wide and <1 m deep, are identified close to some of these scars (Fig. 12b, d). Similar features have also been observed in different fjords in Spitsbergen (Forwick et al., 2009; Baeten et al., 2010). In these fjords, these features have been interpreted to be pockmarks formed by seepage of thermogenic gas and migration of pore water (Forwick et al., 2009). Even if the observed crater-like depressions in the inner Hardangerfjorden are an order of magnitude smaller than the ones observed in Spitsbergen, we follow the interpretation of Forwick et al. (2009) and suggest them to be pockmarks.

Some of the tributary fjords of Hardangerfjorden are shallower than the main fjord and appear as “hanging valleys”, typical for glacial landscapes. At the steep slope down to the main fjord bottom, at the entrance of the tributary fjords, slide scars are commonly found (Fig. 12). Granvinsfjorden, for example, has a water depth of about 210 m before the relief dips down with gradients of ~50° to a level of 760 m water depth in the main Hardangerfjorden system, where a 200 m-wide crater with 30 m-high rims is observed (Figs. 12b, 12c).

Along the submarine fjord flanks, several sediment accumulation features have been identified. These cone-shaped features have previously been mapped by Bellwald et al. (2016), who interpreted them as colluvial fans with heights of 90–440 m, surface gradients of 20–35° and sediment volumes up to 63 × 10^6 m^3. Close to a 100 m long,

250 m wide and 30° steep, fan-shaped deposit, also described by Bellwald et al. (2016) (Fig. 13a, c), we identified lobes with concentric ridges and blocks (Fig. 13a, b). The bathymetric data also show that these features are associated with a series of gullies along the steep fjord flanks and commonly they are deposited close to the scars identified in the fjord sea floor (Figs. 12, 13).

5. Discussion

5.1. Local and regional MTDs and their location of initiation

The upper seismic unit of Hardangerfjorden is characterized by 19 MTDs partly separated by (glaci)marine deposits (Figs. 6, 7), noting that mass transport deposits comprise ~70% of the total fjord sediment infill, ~93% of the HUU deposits and ~83% of the sediments analyzed in the Calypso core. Due to their impressive imprint in the stratigraphy of Hardangerfjorden, the acoustically transparent facies of the six identified meter-sized deposits clearly identifiable in different fjord basins, are interpreted to reflect megaturbidites. Megaturbidites are characterized by their considerable thickness, their extensive surface areas and their large volumes (Cita et al., 1984). Although the lateral extension of these MTDs is limited by the 10 reported fjord-bottom crossing slide scars, they can be seismically correlated for about 40 km in different fjord basins (Fig. 6). Their transport seems to have occurred along high-amplitude continuous reflections, probably acting as basal surfaces, named basal shear surfaces in Bull et al. (2009).

The origin of MTDs as well as their timing is crucial points in evaluating the main trigger mechanisms for the different events. Following the reflections at the top of each identified MTD across the fjord basins, we observe that multidirectional slide wedges (Fig. 8) and basin-wide mass failures (Figs. 6, 7) occur below the acoustically transparent facies. These slide wedges are deposited along the steeper lateral fjord flanks

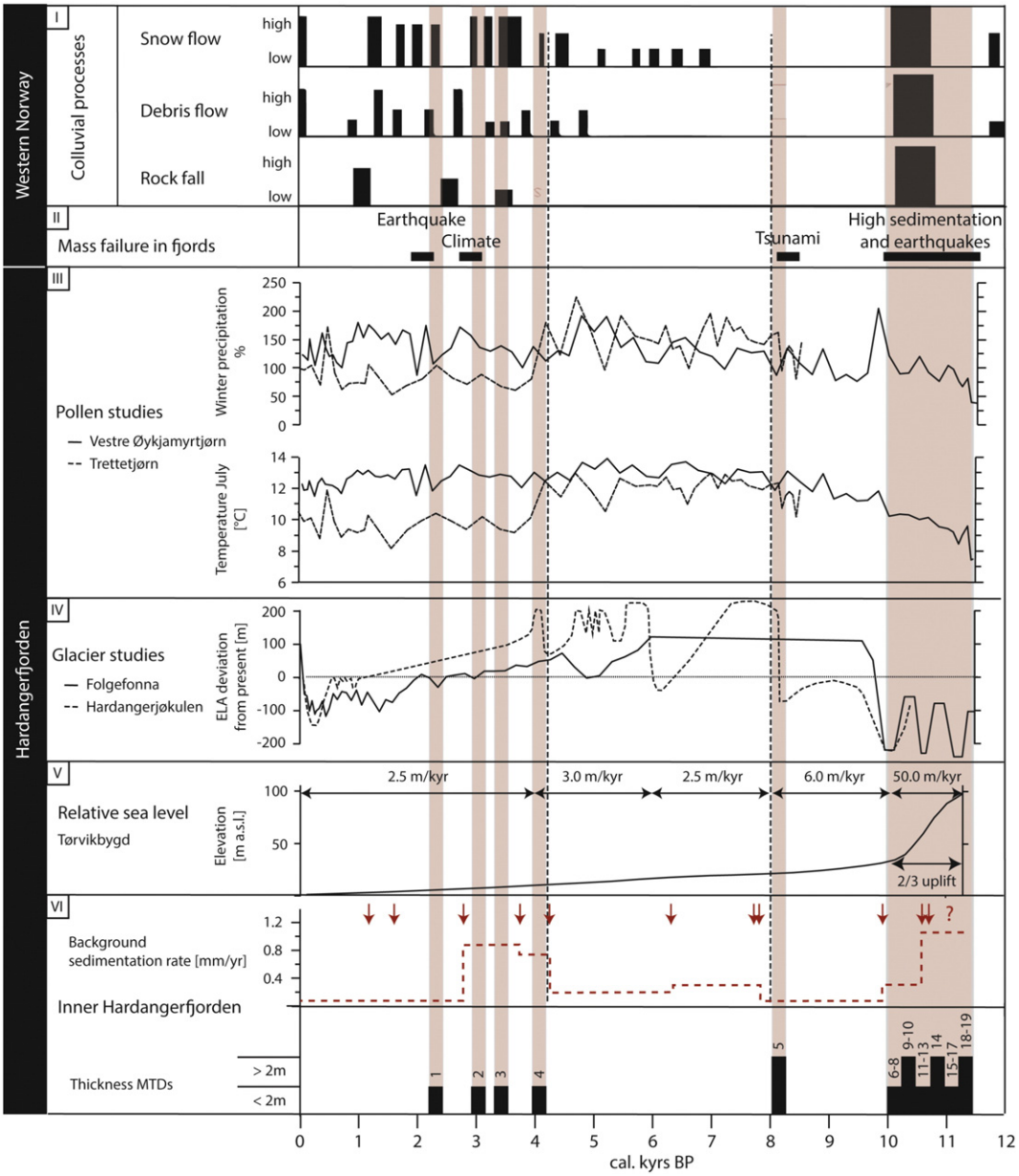

Fig. 14. Correlation of Inner Hardangerfjorden event stratigraphy (lower panel) with other studies, focusing on potential trigger mechanisms. I) Colluvial processes from Blikra and Nemec (1998); II) Mass failure in Western Norwegian fjords modified after Bøe et al. (2004); III) Pollen studies from Bjune et al. (2005); IV) Glacier studies from Bakke et al. (2005) and Dahl and Nesje (1996); V) Relative sea level studies from Romundset et al. (2010). VI) This study: Identified MTDs, background sedimentation rate and position of radiocarbon datings (red arrows).

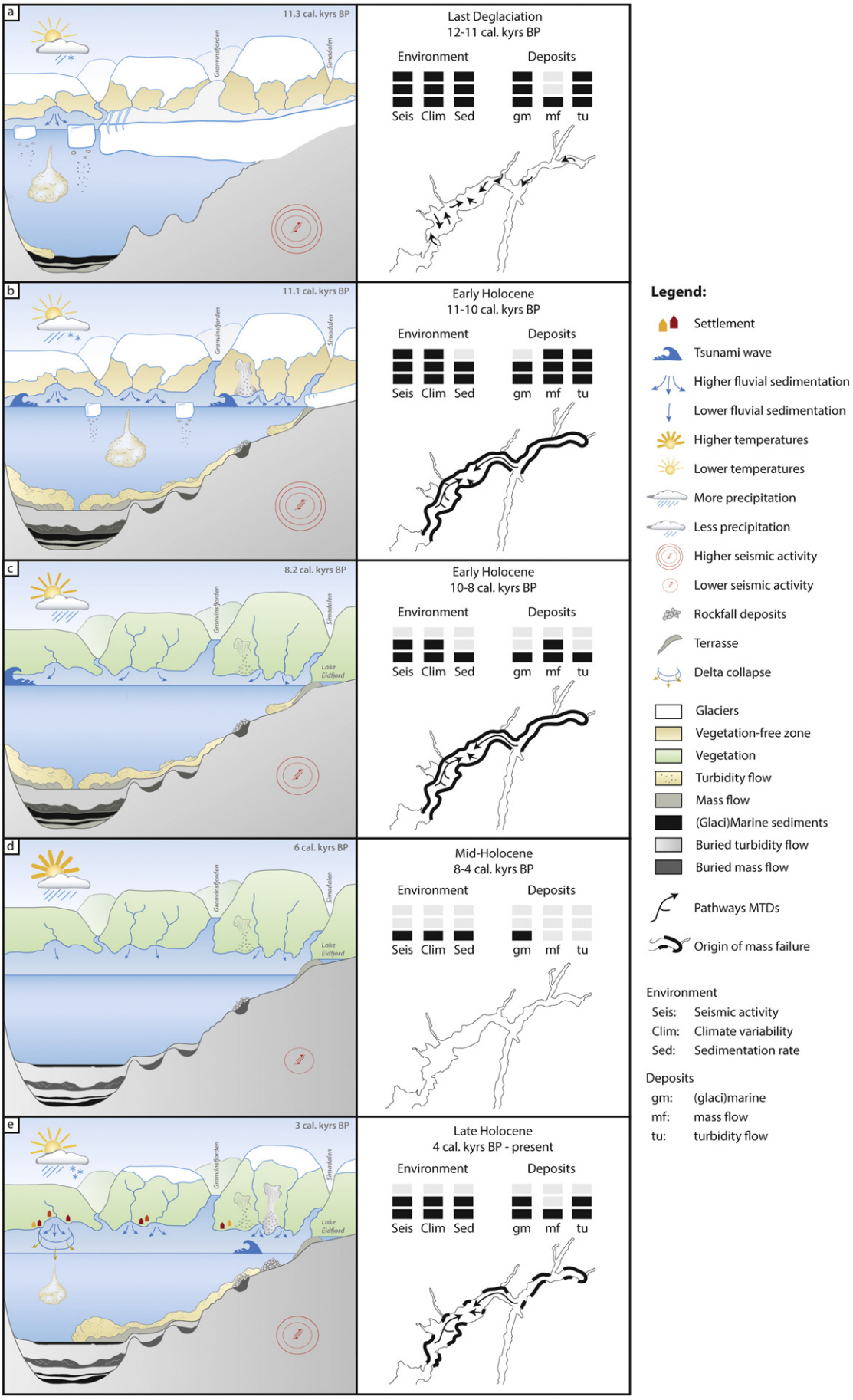
a
11.3 cal. kyrs BP
Granvinsfjorden
Simadalen
Last Deglaciation
12-11 cal. kyrs BP
Environment
Deposits
Seis Clim Sed
gm mf tu
b
11.1 cal. kyrs BP
Granvinsfjorden
Simadalen
Early Holocene
11-10 cal. kyrs BP
Environment
Deposits
Seis Clim Sed
gm mf tu
c
8.2 cal. kyrs BP
Granvinsfjorden
Simadalen
Lake Eidfjord
Early Holocene
10-8 cal. kyrs BP
Environment
Deposits
Seis Clim Sed
gm mf tu
d
6 cal. kyrs BP
Granvinsfjorden
Simadalen
Lake Eidfjord
Mid-Holocene
8-4 cal. kyrs BP
Environment
Deposits
Seis Clim Sed
gm mf tu
e
3 cal. kyrs BP
Granvinsfjorden
Simadalen
Lake Eidfjord
Late Holocene
4 cal. kyrs BP - present
Environment
Deposits
Seis Clim Sed
gm mf tu
Legend:
Settlement
Tsunami wave
Higher fluvial sedimentation
Lower fluvial sedimentation
Higher temperatures
Lower temperatures
More precipitation
Less precipitation
Higher seismic activity
Lower seismic activity
Rockfall deposits
Terrasse
Delta collapse
Glaciers
Vegetation-free zone
Vegetation
Turbidity flow
Mass flow
(Glaci)Marine sediments
Buried turbidity flow
Buried mass flow
Pathways MTDs
Origin of mass failure
Environment
Seis: Seismic activity
Clim: Climate variability
Sed: Sedimentation rate
Deposits
gm: (glaci)marine
mf: mass flow
tu: turbidity flow

or are onlapping the slide scars of the flat fjord basins. Based on these observations, we infer a regional trigger mechanism for nine of the identified MTDs (Table 2), remobilizing sediment volumes of 9×10^6–383×10^6 m^3. Local trigger mechanisms are more likely if an MTD is characterized by a local wedge, but still characterized by a basin-wide turbidite. As our seismic grid is not covering the entire fjord and a regional trigger mechanism could also just trigger local mass failure, we suggest a local or regional trigger mechanism for the other 10 mapped MTDs. These MTDs are only associated with local slide wedges and have volumes of 4×10^6–56×10^6 m^3 (Fig. 9, Table 2).

Large differences in thickness of the HUU between the deepest part of Samlafjorden (max. 53 m) and the steeper and shallower Eidfjorden (max. 15 m) suggest that heavily sediment-loaded turbidity currents from Eidfjorden may repeatedly have been flowing into Samlafjorden and that thresholds in the fjord bottom did not act as complete barriers for the turbidity flows (Fig. 5). This correlates with observations of Holtedahl (1975), who also interpreted Samlafjorden as the final sink for turbidity currents originating in Eidfjorden. We note, however, that the acoustically chaotic facies of MTD3 and MTD4 are only identified in the western part of Samlafjorden, indicating that the mass failures originating north of Jondal (Figs. 6, 9) and at the delta of River Ænes (Fig. 7), respectively.

The main feature identified at the flat fjord bottom is the 10 slide scars (Fig. 5). As they are generally found in areas with the steepest basin floor gradients (Bellwald et al., 2016), we suggest that slope angle is an important preconditioning factor for the initiation of mass movements in the entire inner Hardangerfjorden system. The steps in the headwall of the scars suggest a retrogressive type of movement, which has also been described from the Norwegian continental margin (e.g. Kvalstad et al., 2005).

Mass movements originating from the steep side walls of the fjord is indicated by several features. Slide scars at the mouth of the Granvinsfjord and Simafjord tributary fjords, which can be directly linked with their mass transport deposits along the flat fjord basin (Fig. 12b), highlight the importance of seafloor gradient on sediment stability. Colluvial erosion into colluvial deposits is observed by the series of gullies with associated cones in the central part of Eidfjorden (Fig. 13a, c). Concentric ridges on one of the identified lobes on the northern side of fjord (Fig. 13b) are interpreted as pressure ridges, typical for a contraction domain in the toe domain of mass wasting (Bull et al., 2009), whereas the blocks observed at the front of the lobe represent boulders with longer outrun, a feature typical for mass movement involving unsorted masses (i.e. Bøe et al., 2003). We suggest that the crater located close to slide scar 8 (Fig. 12b, c) could be a result of high-energy channelized mass transport along steep fjord flanks from Granvinsfjorden, an interpretation that is also supported by the built-up of rims. All the above mentioned deposits correlate with slide scars on the flat fjord bottom (Fig. 13), and thus we suggest a link between mass movement processes related to the steep fjord walls and the initiation of mass movements along the flat fjord bottom.

The interpreted pockmarks in Utnefjorden (Fig. 12) may propose a link between fluid flow pathways and mass failures. They could be formed by seepage of thermogenic gas and migration of pore water, as has been discussed by Forwick et al. (2009) in fjords of Spitsbergen, but also elevated pore pressure caused by falling sea level or fluid migration related to tectonic structures. Overpressure-related processes influencing slope sediment instability have been reported from the Gulf of Mexico by Stigall and Dugan (2010).

5.2. Depositional history, timing of mass movements and trigger mechanisms

The discussion of the depositional history and its implication for our understanding of the mechanisms behind the mass movements in the study area are in the following treated for four time periods: (1) The last deglaciation (11,600–11,100 cal. yrs BP), (2) Early Holocene (11,100–8200 cal. yrs BP), (3) Mid-Holocene (8200–4100 cal. yrs BP) and (4) Late Holocene (4100 cal. yrs BP to present) (Figs. 14, 15).

5.2.1. The last deglaciation (11,600–11,100 cal. yrs BP)

The oldest non-reworked marine sediments in the inner Hardangerfjorden system are dated to 10,652 cal. yrs BP in core GS14-187-03PC, resulting in a suggested age of 10,700 cal. yrs BP for the 5.44-m-thick MTD9 (Fig. 10). With a background sediment thicknesses in the range of about 1 ms(twt) between MTD9 and the upper sequence boundary of HLU (Figs. 6, 7), a sediment velocity of 1500 m/s (Fig. 10) and a sedimentation rate of about 1.1 mm/yr (same as for the time period 10,500–10,600 cal. yrs BP, Fig. 14), the upper sequence boundary of HLU is suggested to have an age of around 11,500 cal. yrs BP. This is probably a maximal age, as we suggest the sedimentation rates to be higher directly after the deglaciation (Cofaigh and Dowdeswell, 2001), reaching values of 100–250 mm/yr in Spitsbergen fjords (Elverhøi et al., 1983; Görlich et al., 1987). If anticipating a sedimentation rate of 2 mm/yr, the upper sequence boundary of the HLU is estimated to be around 11,100 years old at the coring location.

After the ice advance in Younger Dryas, the Fennoscandian Ice Sheet started to retreat from the Huglo-Halsenøy islands (Fig. 1b) around 11,600 cal. yrs BP and reached Eidfjord at about 11,100 cal. yrs BP (Mangerud et al., 2013). The estimated ice sheet retreat rates of about 240 m/yr indicate that the inner Hardangerfjorden may have been partly ice-free in the late Younger Dryas (Fig. 15a), implying that the HLU could represent ice-proximal sedimentation related to an ice margin withdrawal. With a maximum HLU thickness of 105 m and by utilizing sedimentation rates estimated from Spitsbergen fjords (Elverhøi et al., 1983; Görlich et al., 1987), the HLU records 420–1050 years. Adding this time to the proposed 11,100 cal. yrs BP of the HLU/HUU sequence boundary results in an age of 12,200–11,600 years for the base of the HLU, which fits with the deglaciation history of the fjord system (Mangerud et al., 2013).

The anticipated higher sedimentation rates during deglaciation periods (Cofaigh and Dowdeswell, 2001) may have resulted in mass movements and reworking of unstable sediments, which may also explain the 50 acoustically transparent packages identified in the HLU (Fig. 7). The sediment reworking could have been initiated by ice-marginal oscillations, glacitectonic deformation, the influence of waves, depositional oversteepening, the impact of calving ice bergs and earthquakes (Lønne, 1995). The slumping of sediments from the foreslope of a delta or subaqueous moraines is another potential trigger mechanism for the reworking of these acoustically transparent packages (Gilbert et al., 1993). The initiation of the first identified meter-sized MTD of the HUU (MTD19, Figs. 6, 7) seems to have started some 100 years after the beginning of the glacimarine sediment infill in the inner Hardangerfjorden system, when sedimentation rates dropped to a postglacial level, whereas the glacio-isostatic rebound was still at the same gradient (Fig. 14).

Fig. 15. Conceptual model showing depositional environments through postglacial time for the Inner Hardangerfjorden system. Deposits not to scale. (a) Deglaciation (11,300 cal. yrs BP), (b) Earliest Early Holocene Deglaciation (11,100 cal. yrs BP), (c) End of Early Holocene (8200 cal. yrs BP), (d) Mid-Holocene (6000 cal. yrs BP), (e) Late Holocene (3000 cal. yrs BP). Areas vulnerable to slope failure along the coastline (thick black lined), mass transport directions (black arrows) and intensity of environment-related forcing as well as dominating deposits are indicated.

5.2.2. Early Holocene (11,100–8200 cal. yrs BP)

The Early Holocene in the Hardangerfjorden area is climatically characterized by an increase in summer temperature and winter precipitation (Bjune et al., 2005) (Figs. 14, 15b), with glaciers retreating to higher altitudes (Bakke et al., 2005; Dahl and Nesje, 1996). Due to glacioisostatic rebound, the relative sea level was rising with rates of up to 50 m/kyr in the Hardanger area (Romundset et al., 2010). Our study shows that sedimentation rates in the beginning of this period were the highest (1.1 mm/yr) compared with the rest of the Holocene. These sedimentation rates can be explained by high glacio-fluvial sediment input of a still highly glaciated, freshly exposed unstable terrestrial landscape (Fig. 15b), as also has been suggested for Scottish fjords (McIntyre and Howe, 2010). This high sediment supply in a short time probably resulted in fjord slopes vulnerable to mass failures. 15 MTDs (MTD5–19) are identified in the Inner Hardangerfjorden system in the Early Holocene, giving a mass failure recurrence rate of 1/200 years.

Five MTDs, with basin-wide acoustically chaotic facies at their base (MTD9, 10, 14, 18, 19), are estimated to have been deposited in the time interval between 10,600 and 11,100 cal. yrs BP (Table 2). This indicates enhanced regional mass transport activity in the studied fjord system immediately after the Younger Dryas deglaciation. Stacked slide wedges (Figs. 6, 7) in the seismostratigraphy indicate that all the slopes around the fjord were susceptible for mass wasting in the first 1000 years of the Holocene. Repeated slides and sediment transport in the first 1000 years (Fig. 15b) of the Holocene time period have also been mentioned in previous studies of western Norwegian fjords (Bøe et al., 2004), in northern Norwegian fjords (Forwick and Vorren, 2002) and in Svalbard fjords (Forwick and Vorren, 2007). This MTD recurrence probably happened as a response of the landscape to ice removal and glacio-isostatic rebound, and would fit with previous studies concluding that 2/3 of the Holocene sea level rise occurred within the first 1000 years after the ice retreat (Romundset et al., 2010) (Fig. 14).

As tsunamis triggered by offshore mega-slides have the potential to initiate mass failure in shallow marine basins and coastal lakes (Bondevik et al., 1997), they are also candidates for regional mass failure in fjords. With a suggested age of 8200 cal. yrs BP the uppermost identified MTD with basin-wide slide wedges, MTD5 (Figs. 6, 7), correlates with the Storegga tsunami, which is dated to 8100 ± 250 cal. yrs BP (Haflidason et al., 2005; Bondevik et al., 2012). Tsunami deposits related to the Storegga Slide event in western Norway reach onshore elevations of 10–12 m above sea level (Bondevik et al., 2005) and are identified and well described from lakes and terrestrial localities along the coast of mid- and western Norway (e.g. Vasskog et al., 2013). However, as the Storegga Slide could have been triggered by a M7 + earthquake (Bryn et al., 2005), the same earthquake could directly have initiated mass failures in the Hardangerfjorden system.

The appearance of a MTD along the same identified basal reflection and with the same identified top reflection in different sedimentary basins suggests simultaneous mass failures, which is interpreted as a fingerprint of paleoseismic activity in subaquatic archives (e.g. Strasser et al., 2013). This pattern (Figs. 6, 7) is observed for all six identified meter-sized MTDs of Early Holocene age in Hardangerfjorden (MTD5, 9, 10, 14, 18, 19). For the period after the ice retreat in Younger Dryas (11,600–10,000 cal. yrs BP), increased seismicity is related to rapid isostatic uplift, ~20 times higher than today (Fig. 14). Therefore, we suggest that these six MTDs have been triggered by earthquakes, resulting in an earthquake frequency of 1/600 years. An earthquake trigger is further supported by the seismic stratigraphy of the outer Hardangerfjorden (Fig. 7), which is characterized by five meter-sized MTDs with comparable seismic properties as the MTDs in the inner Hardangerfjorden. Ashi et al. (2014) have suggested from studies in subduction zones that large suspension clouds are correlating with large earthquakes. This could partly explain the thick turbiditic tails of the six identified meter-sized MTDs in this time period (Fig. 9a).

The nine Early Holocene MTDs with basin-wide turbidites, but only local slide wedges (MTD6–8, 11–13, 15–17, Fig. 14, Table 2), could be explained by earthquakes as well. However, they could also be caused by local triggers. The fast glacier retreat caused sediment exposure, which may have been eroded by rivers (McIntyre and Howe, 2010). River discharge could have been higher due to warmer and wetter climate (Bjune et al., 2005) (Fig. 14), potentially resulting in higher flood activity. Furthermore, higher activity of colluvial processes around 10–11 cal. kyrs BP (Blikra and Nemec, 1998) may also have initiated submarine mass failure in the fjord. Therefore, rock avalanches initiating submarine mass failure should be considered as trigger mechanism for these nine MTDs as well. Submarine mass failure triggered by rock avalanches, potentially originating in Eidfjorden and causing basin-wide turbidites, could be reflected by some of the identified decimeter-sized MTDs dated to be around 10,500 cal. yrs BP (Table 2, Fig. 13).

In summary, the identified meter-sized MTDs with basin-wide slide wedges at their base are most likely triggered by earthquakes or earthquake-related tsunamis. Earthquakes, rock avalanches, tsunamis and increased river discharge are the most reasonable processes explaining the cause of the nine decimeter-sized MTDs with basin-wide turbidites and only local slide wedges. It should be noted that the Early Holocene mass failure events are prehistoric, for which time period we do not have information about occurrence, local intensities and magnitudes of earthquake forcing.

5.2.3. Mid-Holocene (8200–4100 cal. yrs BP)

The mid-Holocene time period in the Hardangerfjorden region is characterized by the absence of MTDs (Figs. 14, 15d). In their study from northwestern Norway, Bøe et al. (2004) also documented that the mid-Holocene was a quiet period regarding mass failure events. It has been inferred that the mid-Holocene time period was characterized by warm and wet conditions in the study area (Bjune et al., 2005), including a complete meltdown of both the Hardangerjøkulen and Northern Folgefonna ice caps (Bakke et al., 2005; Dahl and Nesje, 1996) (Fig. 14). The relative sea level was rising with rates of 2.5–3.0 m/kyr (Romundset et al., 2010), which is a much lower rate than that found for the Early Holocene. Additionally, the colluvial systems seem to be rather inactive in this period (Blikra and Nemec, 1998). As a consequence, the sediment supply into the fjord system might have been low, which is also supported by sedimentation rates of 0.2–0.3 mm/yr found from our core analyses (Fig. 14). The absence of mass failures in the mid-Holocene time period can therefore be explained by a lower seismic activity related to lower glacioisostactic uplift rates and reduced sediment input.

5.2.4. Late Holocene (4100 cal. yrs BP–present)

The relative sea level rise did not significantly change from the mid-Holocene into the Late Holocene (Romundset et al., 2010) (Fig. 14). The climate was colder in the Late Holocene compared to the mid-Holocene (Bjune et al., 2005) with colder winters and more rainy summers. The glaciers advanced and the colluvial systems were reactivated (Bakke et al., 2005; Dahl and Nesje, 1996; Blikra and Nemec, 1998). The sedimentation rates were quite high in the very earliest parts of the Late Holocene (0.8 mm/yr), but decreased to 0.1 mm/yr during the last 3000 years of the period.

Mass transport in Hardangerfjorden is again documented in the time period between 4100 and 2400 cal. yrs BP in the form of four MTDs (MTD1–4, Figs. 9, 10). Recurrence rates for basin-wide turbiditic depositions in the Late Holocene time period are therefore estimated to 1/1000 years. This indicates that Hardangerfjorden in the Late Holocene represents a more active system regarding mass wasting compared with several other Norwegian fjords (e.g. Bøe et al., 2003; Forwick and Vorren, 2002).

In the outer Hardangerfjorden, Holtedahl (1975) dated a turbidite package to 5608 ± 35 cal. yrs BP. This turbidite can be related to a slump deposit, suggested by Holtedahl (1975) to have been triggered

by a collapse of the River Ænes Delta (Fig. 7a). As the radiocarbon dating material was taken at a level of 10 cm below the erosive turbidite, this turbidite and its associated slump may correlate with the identified local wedge and its associated turbidite layer of MTD4 in Samlafjorden (Figs. 8, 12). Therefore, we suggest seismic shaking as the most likely trigger mechanism for MTD4, which could also have resulted in the River Ænes delta collapse. Similarly to MTD4, MTD3 shows several slide wedges in different fjord basins, and we thus suggest it to be regionally-triggered, potentially by an earthquake as well.

Climate variability and deterioration are documented for the Hardangerfjorden area around 3000 cal. yrs BP (Nesje et al., 1995; Matthews et al., 1997). MTD2, characterized by a basin-wide turbidite and a slide wedge limited to the fjord region north of Jondal (Figs. 9, 11), could therefore be related to exceptional meltwater events, including glacier outbursts or increased ice melt during warm summers. Mulder and Syvitski (1995) and Mulder et al. (2003) studied similar relationships of turbidity currents generated during exceptional discharge on a global scale. As the colluvial systems in Hardangerfjorden were reactivated the Late Holocene (Fig. 14), snow flows, debris flows and rock avalanches should also be considered as trigger mechanisms for this event.

The youngest identified mass transport event in the inner Hardangerfjorden system, MTD1, is dated to 2400 cal. yrs BP (Figs. 9, 10). No associated slide wedge has been identified for this mass failure event (Fig. 9). Mass movements of the same age have also been identified in many fjords and lakes in western Norway, and for which an earthquake has been suggested as the final trigger mechanism (Bøe et al., 2004).

Mass movement events have not been detected since 2400 cal. yrs BP in the Calypso core raised from Samlafjorden. Studies from northwestern Norwegian fjords also suggest a low frequency of subaquatic mass movements for the last 2000 years (Bøe et al., 2004). Even if western Norway is still seismically active (Bungum et al., 2005), these events either have not the energy to result in submarine mass failure or the sediment supply is not high enough to generate basin-wide MTDs. We note that the historically documented M4.5 earthquake with an epicenter at Bømlo (Fig. 1; Hicks and Ottemöller, 2001) did not seem to have triggered any turbidite in the inner part of Hardangerfjorden.

Indicators of colluvial mass movements have been identified at several locations in Eidfjorden, both in the bathymetric records and in the seismic profiles (Fig. 13) (compare also Bellwald et al., 2016). Easily-detectable colluvial deposits indicate ongoing mass wasting in Eidfjorden, and acoustically chaotic facies in the seismic data indicate even larger colluvial mass wasting at the same localities in the past. Based on our present data base, it is not possible to correlate these colluvial deposits to the MTDs identified in the seismic profiles from Eidfjorden and Samlafjorden.

Small-sized mass wasting may be generated during extreme river discharges (Piper et al., 1999). However, heavily sediment-laden rivers are rather responsible for turbidite deposits than slide debrite initiation during floods or glacier outburst events (Bornhold et al., 1994). At present, rivers draining the Hardangerjøkulen and Folgefonna glaciers are the only rivers with glacial-derived discharge (Fig. 1b). Historical glacier outburst-triggered deposits from Hardangerjøkulen Glacier in 1893 and 1937 have been suggested in Simafjorden (Holtedahl, 1975).

5.3. Regional and global constrains

The new insights about the timing and triggering of MTDs in the Inner Hardangerfjorden may have broader implications for other marine and lacustrine settings. Sedimentation rate seems to be the significant preconditioning factor for mass failure in the Hardangerfjorden system. 18 of 19 MTDs have been triggered when background sedimentation rate was >0.3 mm/yr. Sedimentation rates higher than 0.5 mm/yr have been suggested to increase the sensitivity for earthquake as a trigger in lakes in moderately active seismotectonic regions in the Western Alps (Wilhelm et al., 2015). We postulate that an increasing sedimentation rate in Hardangerfjorden may imply an increasing sensitivity for mass failure occurrence in general, but also an increasing sensitivity to seismic shaking in Western Norwegian fjords as well. We further suggest that mass failure did not occur after 2400 cal. yrs BP as sedimentation rates drastically decreased from ~0.8 mm/yr in the time period of 2800–3700 cal. yrs BP to 0.1 mm/yr for the time period of 2800–1200 cal. yrs BP. MTD5, dated to 8200 cal. yrs BP, occurred in a time period when sediment accumulated in rates of ~0.1 mm/yr. We thus suggest a very strong earthquake to have triggered this MTD, which is supported by coevally-triggered MTDs in other Norwegian fjord systems (Bøe et al., 2004) and also discussed for the Storegga Slide (Bryn et al., 2005).

Observations in Swiss lakes show a similar pattern of mass movement activity as found in the Hardangerfjorden system, i.e. high activity in the time period directly after the last glacial retreat, a quiet period in the mid-Holocene, and a renewed period with mass failure activity during the last 4000 years of the Holocene (Strasser et al., 2013). Strasser et al. (2013) suggested strong earthquakes, related to tectonic fracture zones, as the most likely trigger mechanism for the MTDs in the Swiss lakes. Intraplate seismicity in northern Central Europe is largely induced by the melting of the Fennoscandian Ice Sheet, also indicated by faults becoming reactivated due to stress increase in the Late Holocene (Brandnes et al., 2015). Thus there might be a link between stress build-up and periods of stress release and mass movement activity in fjords glaciated in the past. Due to the similarities in the timing of mass movements, the MTDs of the Late Holocene from the inner Hardangerfjorden may be related to a similar stress build-up in the mid-Holocene period.

Stress could potentially be built-up until a critical threshold, which for Northern Central Europe is reached at around 4000 cal. yrs BP (Brandnes et al., 2015). Thus, the low mass failure period in the mid-Holocene in Hardangerfjorden can be either related to stress built-up and low seismic activity or by sediments not sensitive enough to fail due to seismic shaking. This stress-related MTD pattern could thus be observed worldwide in different marine and lacustrine settings with glacial catchments in the past.

Submarine landslides and rock avalanches can both result in tsunamis (Harbitz et al., 2014; Brothers et al., 2016). In some Norwegian fjord systems, rock avalanches exceeding volumes of 10^6 m^3 have been linked with the initiation of destructive tsunamis (Hermanns et al., 2006; Blikra et al., 2006). The rock avalanche deposits identified close to the Hardanger Bridge (Figs. 2c, 13d), comprising a volume of about 30×10^6 m^3, are an order of magnitude larger compared with the rock avalanche deposits identified in Nordfjord (Lyså et al., 2009), for which a tsunami wave of up to tens of meters has been suggested. A 62 m-high tsunami triggered by a rock avalanche with a volume of 3×10^6 m^3 hit Tafjord in 1934 (Blikra et al., 2006). Tsunami simulations from the movement of a rock volume of 30–40 $\times 10^6$ m^3 in the Åknes area in Geirangerfjorden resulted in wave run-ups of up to ~80 m (www.ngi.no). Comparing these volumes with our study site, the observed rock avalanche nearby the Hardanger Bridge may have triggered a several meter high tsunami. However, the volumes of the submarine mass movements of Hardangerfjorden are even an order of magnitude larger than the rock avalanche deposits, comprising volumes of 383×10^6 m^3 for the largest MTD (Table 2). A devastating tsunami, triggered by the destabilization of 700×10^6 m^3 of sediment in a submarine landslide complex, hit the village of Chenega in southern Alaska in 1964 (Brothers et al., 2016). Similarly, devastating tsunamis may have resulted from some of the submarine triggered MTDs in Hardangerfjorden.

6. Conclusions

High-resolution acoustic data and information obtained from a 15.7-m-long Calypso sediment core as well as high-resolution information

from studies on climate, colluvial systems, glaciation history and uplift history, have increased our understanding about mass transport deposits, mass movement trigger mechanisms, mass movement recurrence rates as well as depositional environments within high-latitude fjord systems. The following conclusions can be drawn from this study:

- Two main seismic units have been identified in the inner Hardangerfjorden system: A lower, up to 100 m thick, glacimarine unit (HLU) suggested to be of Younger Dryas age, and a <55 m thick upper unit (HUU), dominated by 19 postglacial MTDs.
- 10 slide scars and colluvial deposits expressed in the fjord bottom document that a highly dynamic depositional environment existed in the Hardangerfjorden system during the postglacial period.
- The postglacial mass movement history has been split into three separate periods:
  - The Early Holocene (11,100–8200 cal. yrs BP) is characterized by six regionally-triggered and nine regionally- or locally-triggered MTDs. This high activity is suggested to be caused by glacioisostatic uplift-related earthquakes, rock avalanches, earthquake-related/rock-avalanche-related tsunamis or climatic and colluvial processes.
  - The mid-Holocene (8200–4100 cal. yrs BP) was a quiet period with respect to mass movements, probably due to a combination of lower sedimentation rates and low seismic activity.
  - Submarine mass wasting was reactivated in the Late Holocene (4100 cal. yrs BP to present). Three MTDs identified in this period are suggested to have a regional trigger mechanism, which could be related to release of stress built up during the mid-Holocene. One MTD is suggested to have a local or regional trigger mechanism, including climatic processes, rock avalanches and rock-avalanche-related tsunamis.

- One of the identified Early Holocene MTDs (MTD5), with a suggested age of 8246 ± 202 cal. yrs BP and with a sediment volume of 0.2 km^3, indicates that processes related to the large submarine Storegga Slide event might have impacted the Inner Hardangerfjorden system.
- Postglacial mass movement recurrence intervals for Hardangerfjorden are estimated to be 1/200 yrs in the Early Holocene and 1/1000 yrs for the Late Holocene.
- Since 2400 cal. yrs BP the Hardangerfjorden system has, similarly with many other Norwegian fjords, not been impacted by large mass failures. The absence of mass movements may be related to the observed low sedimentation rates.
- The MTDs have been identified in time periods of high sedimentation rates, whereas they have not been observed in time periods characterized by low sedimentation rates. We thus suggest that sediment supply highly affects the sensitivity of sediment for mass failure. Regionally-triggered events might therefore not always be recorded in the sediments of the fjord.

Acknowledgements

We acknowledge Statnett and DOF Subsea Norway AS for access to high-resolution bathymetric data. Atle Nesje, Jostein Bakke, Jan Mangerud, John Inge Svendsen, Inge Aarseth, Matthias Forwick, Flavio Anselmetti and Michael Strasser are all thanked for valuable discussions and comments. We also acknowledge Dag Inge Blindheim, Tobias Schwestermann, Jannicke Kuvås and Daniel Wiberg for helping in laboratory and with the seismic data. Irka Hajdas is thanked for advice and ^{14}C AMS datings. We are grateful for the help with visualization issues and age models to Eva Bjørseth and Lukas Becker, respectively. The captains and crews onboard R/V G.O. Sars are acknowledged for all the help during UiB research cruises GS14-186 and GS14-187. The research leading to these results has received funding from the People Programme (Marie Curie Actions) of the European Union's Seventh Framework Programme FP7/2007-2013/ under REA grant agreement no. 317217. The research forms part of the GLANAM (GLAciated North Atlantic Margins) Initial Training Network. We further thank the two anonymous reviewers for detailed and constructive comments.

References

Aarseth, I., 1997. Western Norwegian fjord sediments: age, volume, stratigraphy, and the role as temporary depository during glacial cycles. Mar. Geol. 143, 39–53.
Aarseth, I., Lønne, Ø., Giskeødegaard, O., 1989. Submarine slides in glaciomarine sediments in some western Norwegian fjords. Mar. Geol. 88, 1–21.
Alfaro, E., Holz, M., 2014. Seismic geomorphological analysis of deepwater gravity-driven deposits on a slope system of the southern Colombian Caribbean margin. Mar. Pet. Geol. 57, 294–311.
Ashi, J., Sawada, R., Omura, A., Ikehara, K., 2014. Accumulation of an earthquake-induced extremely turbid layer in a terminal basin of the Nankai accretionary prism. Earth, Planets and Space 66, 51.
Baeten, N.J., Forwick, M., Vogt, C., Vorren, T.O., 2010. Late Weichselian and Holocene sedimentary environments and glacial activity in Billefjorden, Svalbard. In: Howe, J.A., Austin, W.E.N., Forwick, M., Paetzel, M. (Eds.), Fjord Systems and Archives. Geological Society, London, Special Publications vol. 344, pp. 207–223.
Bakke, J., Lie, Ø., Nesje, A., Dahl, S.O., Paasche, Ø., 2005. Utilizing physical sediment variability in glacier-fed lakes for continuous glacier reconstructions during the Holocene, northern Folgefonna, western Norway. The Holocene 15 (2), 161–176.
Bellwald, B., Hjelstuen, B.O., Sejrup, H.P., Haflidason, H., 2016. Postglacial mass failures in the Inner Hardangerfjorden system, Western Norway. In: Lamarche, G., et al. (Eds.), Submarine Mass Movements and Their Consequences, Advances in Natural and Technological Hazard Research, pp. 73–82.
Bjune, A.E., Bakke, J., Nesje, A., Birks, H.J.B., 2005. Holocene mean July temperature and winter precipitation in western Norway inferred from palynological and glaciological lake-sediment proxies. The Holocene 15 (2), 177–189.
Blaaw, M., Christen, J.A., 2011. Flexible paleoclimate age-depth models using an autoregressive gamma process. Bayesian Anal. 6, 457–474.
Blikra, L.H., Nemec, W., 1998. Postglacial colluvium in western Norway: depositional processes, facies and palaeolicmatic record. Sedimentology 45, 909–959.
Blikra, L.H., Longva, O., Braathen, A., Anda, E., Dehls, J.F., Stalsberg, K., 2006. Rock slope failures in Norwegian fjord areas: examples, spatial distribution and temporal pattern. In: Evans, S.G., Scarawcia Mugnozza, G., Strom, A.L., Hermanns, R.L. (Eds.), Landslides from Massive Rock Slope Failure. Nato Science Series IV, Earth and Environmental Sciences vol. 49, pp. 475–496.
Bøe, R., Rise, L., Blikra, L.H., Longva, O., Eide, A., 2003. Holocene mass-movement processes in Trondheimsfjorden, Central Norway. Nor. J. Geol. 83, 3–22.
Bøe, R., Longva, O., Lepland, A., Blikra, L.H., Sønstegaard, E., Haflidason, H., Bryn, P., Lien, R., 2004. Postglacial mass movements and their causes in fjords and lakes in western Norway. Nor. J. Geol. 84, 35–55.
Bondevik, S., Svendsen, J.I., Mangerud, J., 1997. Tsunami sedimentary facies deposited by the Storegga tsunami in shallow marine basins and coastal lakes, western Norway. Sedimentology 44, 1115–1131.
Bondevik, S., Løvholt, F., Harbitz, C., Mangerud, J., Dawson, A., Svendsen, J.I., 2005. The Storegga Slide tsunami - comparing field observations with numerical simulations. Mar. Pet. Geol. 22, 195–208.
Bondevik, S., Stormo, S.K., Skjerdal, G., 2012. Green mosses date the Storegga tsunami to the chilliest decades of the 8.2 ka cold event. Quat. Sci. Rev. 45, 1–6.
Bornhold, B.D., Ren, P., Prior, D.B., 1994. High-frequency turbidity currents in British Columbia fjords. Geo-Mar. Lett. 14, 238–243.
Brandnes, C., Steffen, H., Steffen, R., Wu, P., 2015. Intraplate seismicity in northern Central Europe is induced by the last glaciation. Geology 43 (7), 611–614.
Bronk Ramsey, C., 2013. OxCal v4.2.4.
Brothers, D.S., Haeussler, P.J., Liberty, L., Finlayson, D., Geist, E., Labay, K., Byerly, M., 2016. A submarine landslide source for the devastating 1964 Chenega tsunami, southern Alaska. Earth Planet. Sci. Lett. 438, 112–121.
Bryn, P., Berg, K., Forsberg, C.F., Solheim, A., Kvalstad, T.J., 2005. Explaining the Storegga Slide. Mar. Pet. Geol. 22, 11–19.
Bull, S., Cartwright, J., Huuse, M., 2009. A review of kinematic indicators from mass-transport complexes using 3D seismic data. Mar. Pet. Geol. 26, 1132–1151.
Bungum, H., Lindholm, C., Faleide, J.I., 2005. Postglacial seismicity offshore mid-Norway with emphasis on spatio-temporal-magnitudal variations. Mar. Pet. Geol. 22, 137–148.
Cita, M.B., Camerlenghi, A., Rimoldi, B., 1984. Deep-sea tsunami deposits in the eastern Mediterranean: new evidence and depositional models. Sediment. Geol. 104, 155–173.
Cofaigh, C.Ó., Dowdeswell, J.A., 2001. Laminated sediments in glacimarine environments: diagnostic criteria for their interpretation. Quat. Sci. Rev. 20, 1411–1436.
Dahl, S.O., Nesje, A., 1996. A new approach to calculating Holocene winter precipitation by combining glacier equilibrium-line altitude and pine-tree limits: a case study from Hardangerjøkulen, central southern Norway. The Holocene 6 (4), 381–398.
Elverhøi, A., Lønne, Ø., Seland, R., 1983. Glaciomarine sedimentation in a modern fjord environment, Spitsbergen. Polar Res. 1, 127–149.
Forwick, M., Vorren, T.O., 2002. Deglaciation history and post-glacial mass movements in Balsfjord, northern Norway. Polar Res. 21, 259–266.
Forwick, M., Vorren, T.O., 2007. Holocene mass-transport activity and climate in outer Isfjorden, Spitsbergen: marine and subsurface evidence. The Holocene 17 (6), 707–716.

Forwick, M., Baeten, N.J., Vorren, T.O., 2009. Pockmarks in Spitsbergen fjords. Nor. J. Geol. 89, 65–77.
Gilbert, R., Aitken, A.E., Lemmen, D.S., 1993. The glacimarine sedimentary environment of Expedition Fiord, Canadian High Arctic. Mar. Geol. 110, 257–273.
Görlich, K., Weslawski, J.M., Zajaczkowski, M., 1987. Suspension settling effect on macrobenthos biomass distribution in the Hornsund fjord, Spitsbergen. Polar Res. 5, 175–192.
Haeussler, P., Leith, W., Wald, D., Filson, J., Wolfe, C., Applegate, D., 2014. Geophysical advances triggered by 1964 Great Alaska Earthquake. Eos 95, 141–142.
Haflidason, H., Lien, R., Sejrup, H.P., Forsberg, C.F., Bryn, P., 2005. The dating and morphology of the Storegga Slide. Mar. Pet. Geol. 22, 123–136.
Hansbo, S., 1957. A new approach to the determination of the shear strength of clay by the fall-cone test. Royal Swedish Geotechnical Institute Proceedings 14, 5–47.
Harbitz, C.B., Løvholt, F., Bungum, H., 2014. Submarine landslide tsunamis: how extreme and how likely? Nat. Hazards 72 (3), 1341–1374.
Hermanns, R.L., Blikra, L.H., Naumann, M., Nilsen, B., Panthi, K.K., Stromeyer, D., Longva, O., 2006. Examples of multiple rock-slope collapses from Köfels (Ötz valley, Austria) and western Norway. Eng. Geol. 83, 94–108.
Hicks, E.C., Ottemöller, L.R., 2001. The ML 4.5 Stord/Bømlo, southwestern Norway, earthquake of 12 August 2000. Nor. J. Geol. 81, 293–304.
Hjelstuen, B.O., Brendryen, J., 2014. Submarine mass movements and trigger mechanisms in Byfjorden, western Norway. In: Krastel, S., Behrmann, J.H., Völker, D., Stipp, M., Berndt, C., Urgeles, R., Chaytor, J., Huhn, K., Strasser, M., Harbitz, C.B. (Eds.), Submarine Mass Movements and Their Consequences. Advances in Natural and Technological Hazard Research vol. 37, pp. 351–359.
Hjelstuen, B.O., Kjennbakken, H., Bleikli, V., Ersland, R.A., Kvilhaug, S., Euler, C., Alvheim, S., 2013. Fjord stratigraphy and processes – evidence from the NE Atlantic Fensfjorden system. J. Quat. Sci. 28, 421–432.
Holtedahl, H., 1975. The geology of the Hardangerfjord, West Norway. Nor. Geol. Unders. 323, 1–87.
Howe, J.A., Austin, W.E.N., Forwick, M., Paetzel, M., Harland, R., Cage, A.G., 2010. Fjord systems and archives: a review. Geol. Soc. Lond., Spec. Publ. 344, 5–15.
Hughes Clarke, J.E., Vidiera Marques, C.R., Pratomo, D., 2014. Imaging active mass-wasting and sediment flows on a Fjord Delta, Squamish, British Columbia. In: Krastel, S., Behrmann, J.H., Völker, D., Stipp, M., Berndt, C., Urgeles, R., Chaytor, J., Huhn, K., Strasser, M., Harbitz, C.B. (Eds.), Submarine Mass Movements and Their Consequences. Advances in Natural and Technological Hazards Research vol. 37, pp. 249–260.
Kvalstad, T.J., Andresen, L., Forsberg, C.F., Berg, K., Bryn, P., Wangen, M., 2005. The Storegga slide: evaluation of triggering sources and slide mechanics. Mar. Pet. Geol. 22, 245–256.
L'Heureux, J.S., Hansen, L., Longva, O., Emdal, A., Grande, L.O., 2010. A multidisciplinary study of submarine landslides at the Nidelva fjord delta, Central Norway – implications for geohazard assessment. Nor. J. Geol. 90, 1–20.
Lønne, I., 1995. Sedimentary facies and depositional architecture of ice-contact glaciomarine systems. Sediment. Geol. 98, 13–43.
Lyså, A., Hjelstuen, B.O., Larsen, E., 2009. Fjord infill in a high-relief area: rapid deposition influenced by deglaciation dynamics, glacio-isostatic rebound and gravitational activity. Boreas 39, 39–55.
Mangerud, J., Goehring, B.M., Lohne, Ø.S., Svendsen, J.I., Gyllencreutz, R., 2013. Collapse of marine-based outlet glaciers from the Scandinavian Ice Sheet. Quat. Sci. Rev. 67, 8–16.
Matthews, J.A., Dahl, S.O., Berrisford, M.S., Nesje, A., Dresser, P.Q., Dumayne-Peaty, L., 1997. A preliminary history of Holocene colluvial (debris-flow) activity, Leirdalen, Jotunheimen, Norway. J. Quat. Sci. 12, 117–129.
McIntyre, K.L., Howe, J.A., 2010. Scottish west coast fjords since the last glaciation: a review. Geol. Soc. Lond., Spec. Publ. 344, 305–329.
Mulder, T., Cochonat, P., 1996. Classification of offshore mass movements. J. Sediment. Res. 66 (1), 43–57.
Mulder, T., Syvitski, J.P.M., 1995. Turbidity currents generated at river mouths during exceptional discharges to world oceans. The Journal of Geology 103 (3), 285–299.
Mulder, T., Syvitski, J.P.M., Migeon, S., Faugères, J.-C., Savoye, B., 2003. Marine hyperpycnal flows: initiation, behavior and related deposits. A review. Mar. Pet. Geol. 20, 861–882.
Nesje, A., Dahl, S.O., Løvlie, R., 1995. Late Holocene glacier and avalanche activity in the Ålfoten area, western Norway: evidence from a lacustrine sedimentary record. Nor. J. Geol. 75, 120–126.
Piper, D.J.W., Cochonat, P., Morrison, M.L., 1999. The sequence of events around the epicentre of the 1929 Grand Banks earthquake: initiation of debris flows and turbidity current inferred from sidescan sonar. Sedimentology 46, 79–97.
Reimer, P.J., Bard, E., Bayliss, A., Beck, J.W., Blackwell, P.G., Ramsey, C.B., Buck, C.E., Cheng, H., Edwards, R.L., Friedrich, M., Grootes, P.M., Guilderson, T.P., Haflidason, H., Hajdas, I., Hatte, C., Heaton, T.J., Hoffmann, D.L., Hogg, A.G., Hughen, K.A., Kaiser, K.F., Kromer, B., Manning, S.W., Niu, M., Reimer, R.W., Richards, D.A., Scott, E.M., Southon, J.R., Staff, R.A., Turney, C.S.M., van der Plicht, J., 2013. Intcal13 and Marine13 radiocarbon age calibration curves, 0–50000 years cal BP. Radiocarbon 55, 1869–1887.
Romundset, A., Lohne, Ø.S., Mangerud, J., Svendsen, J., 2010. The first Holocene relative sea-level curve from the middle part of Hardangerfjorden, western Norway. Boreas 39, 87–104.
Schnellmann, M., Anselmetti, F.S., Giardini, D., McKenzie, J.A., 2005. Mass movement-induced fold-and-thrust belt structures in unconsolidated sediments in Lake Lucerne. Sedimentology 52, 271–289.
Stigall, J., Dugan, B., 2010. Overpressure and earthquake initiated slope failure in the Ursa region, northern Gulf of Mexico. J. Geophys. Res. 115, 167–178.
St-Onge, G., Chapron, E., Mulsow, S., Salas, M., Viel, M., Debret, M., Foucher, A., Mulder, T., Winiarski, T., Desmet, M., Costa, P.J.M., Ghaleb, B., Jaouen, A., Locat, J., 2012. Comparison of earthquake-triggered turbidites from the Saguenay (Eastern Canada) and Reloncavi (Chilean margin) Fjords: implications for paleoseismicity and sedimentology. Sediment. Geol. 243-244, 89–107.
Strasser, M., Monecke, K., Schnellmann, M., Anselmetti, F.S., 2013. Lake sediments as natural seismographs: a compiled record of Late Quaternary earthquakes in Central Switzerland and its implication for Alpine deformation. Sedimentology 60, 319–341.
Sumner, E.J., Siti, M.I., McNeill, L.C., Talling, P.J., Henstock, T.J., Wynn, R.B., Djajadihardja, Y.S., Permana, H., 2013. Can turbidites be used to reconstruct a paleoearthquake record for the central Sumatran margin? Geology 41, 763–766.
Syvitski, J.P.M., Burrell, D.C., Skei, J.M., 1987. Fjords – Processes and Products. Springer, New York (379 pp).
Van Daele, M., Versteeg, W., Pino, M., Urrutia, R., De Batist, M., 2013. Widespread deformation of basin-plain sediments in Aysén fjord (Chile) due to impact of earthquake-triggered, onshore-generated mass movements. Mar. Geol. 337, 67–79.
Vasskog, K., Waldmann, N., Bondevik, S., Nesje, A., Chapron, E., Ariztegui, D., 2013. Evidence for Storegga tsunami run-up at the head of Nordfjord, western Norway. J. Quat. Sci. 28 (4), 391–402.
Wilhelm, B., Nomade, J., Crouzet, C., Litty, C., Sabatier, P., Belle, S., Rolland, Y., Revel, M., Courboulex, F., Arnaud, F., Anselmetti, F.S., 2015. Quantified sensitivity of small lake sediments to record historic earthquakes: implications for paleoseismology. J. Geophys. Res. Earth Surf. 121, 2–16.
www.geonorge.no, Kartverket, The Norwegian Mapping Authority, Hønefoss, Norway, 25.11.2014.
www.ngi.no, Norges Geotekniske Institutt (NGI), Norwegian Geotechnical Institute, Oslo, Norway, 15.03.2016.
www.nve.no, Norges vassdrags- og energidirektorat (NVE), Norwegian Water Resources and Energy Directorate, Oslo, Norway, 10.12.2014.
www.ssb.no, Statistik sentralbryå, Statistics Norway, Oslo, Norway, 27.08.2015.